Elsevier Editorial System(tm) for Materials Characterization
Manuscript Draft

Manuscript Number:

Title: IDENTIFICATION OF SIGMA AND CHI PHASES IN DUPLEX STAINLESS STEELS

Article Type: Technical Paper

Keywords: Duplex Stainless Steel; Superduplex Stainless Steel; Sigma-phase; Chi-phase; Ageing; Phase Transformations.

Corresponding Author: Prof. Nuria LLORCA-ISERN, PhD

Corresponding Author's Institution: Universitat de Barcelona

First Author: Nuria LLORCA-ISERN, PhD

Order of Authors: Nuria LLORCA-ISERN, PhD; Hector LOPEZ-LUQUE; Isabel LOPEZ-JIMENEZ; Maria Victoria BIEZMA, PhD

Abstract: The aim of this work is to find out the most suitable method for detecting and analyzing accurately the formation conditions of secondary phases, particularly Sigma-phase (σ-phase) and Chi-phase (χ-phase) in duplex stainless steels (UNS S32205 and UNS S32750). The microstructure was characterized after a solution annealing at 1080oC followed by an isothermal heating at 830oC for different time ranges, ranging from 1 minute to 9 hours, in order to enlighten the controversial point concerning the mechanism of χ-phase nucleation in relation with the σ-phase. Etched samples were observed using optical microscopy (MO), and scanning electron microscopy (FESEM) with a backscattered electron detector (BSE) was used on unetched samples. Compositional microanalysis (EDS) was carried out for identifying the different phases present in the steels. Sigma phase was easily observed using different etching procedures, whereas χ-phase was only clearly detected with FESEM-BSE on unetched samples. The compositional analyses showed that the molybdenum content in χ-phase almost doubles the content of this element in σ-phase, and as a result the kinetics of nucleation and growth were also found to be remarkably faster when the alloy content in the steel is higher. In addition, chromium nitrides and carbides were also observed to precipitate as a result of the heat treatments and, in the case of the chromium nitrides, they act as a favorable site for the nucleation of σ-phase and χ-phase.

Suggested Reviewers: Paul R Munroe
School of Materials Science & Engineering, University of New South Wales
p.munroe@unsw.edu.au
Expert in microstructure-property relationships in advanced engineering materials.

Heung Nam Han
Materials Science and Engineering, Seoul National University
hnhan@snu.ac.kr
Expert in Metallic materials, Micro-Mechanics and materials processing.

Emel Taban
Mechanical Engineering, Kocaeli University
emelt@kocaeli.edu.tr

Expert in Base Metal and Welded Joints.

Luiz Carlos Casteletti
Materials, Aeronautical and Automitive Engineering, University of Sao Paulo
castelet@sc.usp.br
Expert in duplex stainless steels.

COVER LETTER

The aim of the study was to find the best characterization technique to correctly assess the microstructural changes that occur when duplex steels are affected by high temperature (welding, local T increase...). Although the precipitation of the intermetallic sigma-phase has been widely studied, other phases involved in the process such as chi-phase, nitrides and carbides have not been fully investigated. In the present study, we tested different metallographic etching reagents and compared optical microscopy with the observation by high resolution scanning electron microscopy, the best method resulting to be the FESEM in backscattered electron mode on unetched samples. Identification and characterization of the different phases using compositional analyses (EDS and WDS) allowed us to explain their formation and growth mechanism. Additionally, we also compared the microstructure evolution between a duplex and a superduplex steel.

Adjusting to the content of Materials Characterization, we focused our study on describing the mechanism involved in the precipitation of sigma-phase and chi-phase, characterizing the different phases present in the steels and comparing the alterations occurred in their microstructure.

Núria LLorca-Isern

Héctor López-Luque

Isabel López-Jiménez

Maria Victoria Biezma

*Title Page

IDENTIFICATION OF SIGMA AND CHI PHASES IN DUPLEX STAINLESS STEELS

Information Authors:

NÚRIA LLORCA-ISERN, CPCM Departament de Ciència dels Materials i Enginyeria Metal·lurgica, Facultat de Química, Universitat de Barcelona, Marti-Franqués 1, 08028 Barcelona, Spain, +34934021111, nullorca@ub.edu.

HÉCTOR LÓPEZ-LUQUE, CPCM Departament de Ciència dels Materials i Enginyeria Metal·lurgica, Facultat de Química, Universitat de Barcelona, Marti-Franqués 1, 08028 Barcelona, Spain, +34934021111, hlopezlu7@alumnes.ub.edu

I*SABEL LÓPEZ-JIMÉNEZ*, CPCM Departament de Ciència dels Materials i Enginyeria Metal·lurgica, Facultat de Química, Universitat de Barcelona, Marti-Franqués 1, 08028 Barcelona, Spain, +34934021111, ilopezji9@alumnes.ub.edu

MARIA VICTORIA BIEZMA Department of Earth, Materials Science and Engineering, University of Cantabria - UC, Gamazo, 1, 39004 Santander, Spain, +34942201325, maria.biezma@unican.es

ABSTRACT

The aim of this work is to find out the most suitable method for detecting and analyzing accurately the formation conditions of secondary phases, particularly Sigma-phase (σ-phase) and Chi-phase (χ-phase) in duplex stainless steels (UNS S32205 and UNS S32750). The microstructure was characterized after a solution annealing at 1080oC followed by an isothermal heating at 830oC for different time ranges, ranging from 1 minute to 9 hours, in order to enlighten the controversial point concerning the mechanism of χ-phase nucleation in relation with the σ-phase. Etched samples were observed using optical microscopy (MO), and scanning electron microscopy (FESEM) with a backscattered electron detector (BSE) was used on unetched samples. Compositional microanalysis (EDS) was carried out for identifying the different phases present in the steels. Sigma phase was easily observed using different etching procedures, whereas χ-phase was only clearly detected with FESEM-BSE on unetched samples. The compositional analyses showed that the molybdenum content in χ-phase almost doubles the content of this element in σ-phase, and as a result the kinetics of nucleation and growth were also found to be remarkably faster when the alloy content in the steel is higher. In addition, chromium nitrides and carbides were also observed to precipitate as a result of the heat treatments and, in the case of the chromium nitrides, they act as a favorable site for the nucleation of σ-phase and χ-phase.

GRAPHICAL ABSTRACT

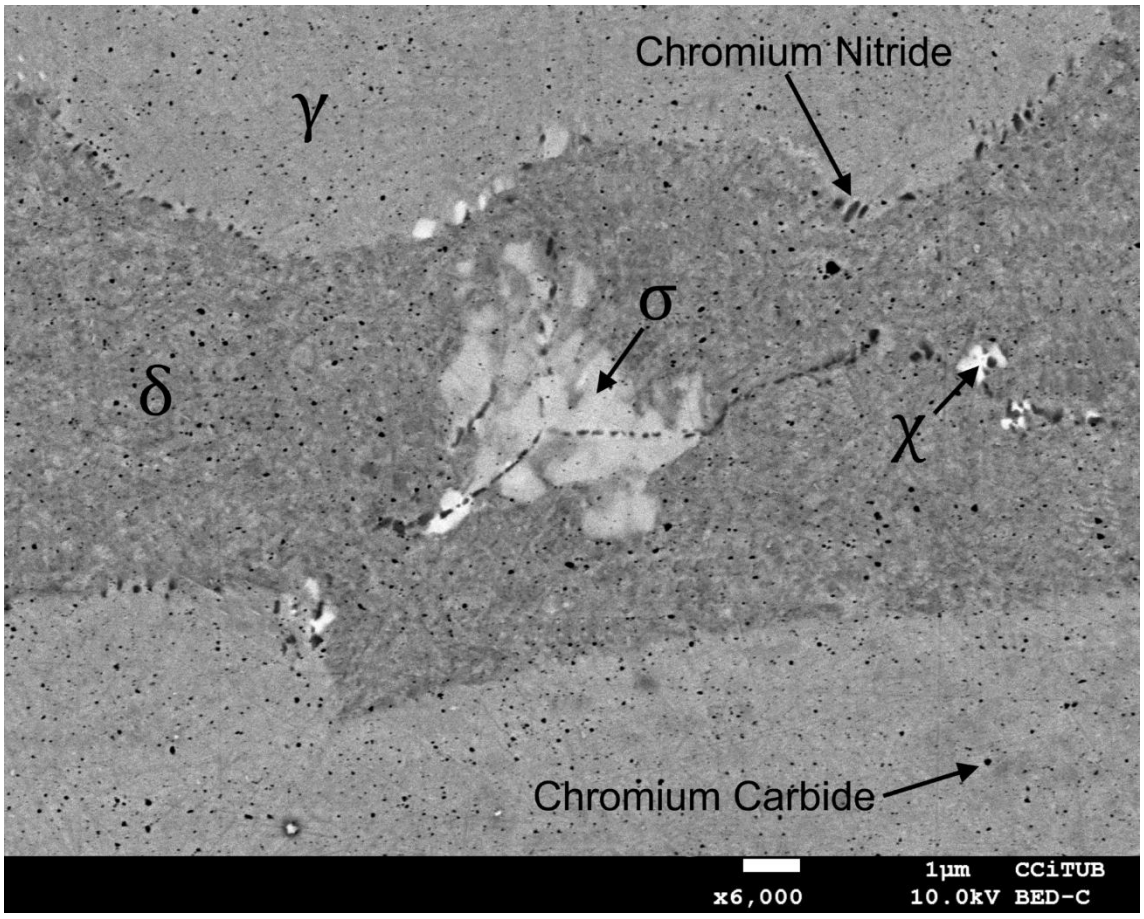

HIGHLIGHTS

Microscopy was used on heat treated duplex steels for microstructure identification.

FESEM-BSE observation on unetched samples provided the best contrast between phases.

Analyses of carbides, nitrides, chi and sigma phases were possible by EDS and WDS.

Chromium nitrides act as favorable site for the nucleation of chi and sigma phases.

Secondary phases nucleation kinetics are faster in superduplex than in duplex steels.

IDENTIFICATION OF SIGMA AND CHI PHASES IN DUPLEX STAINLESS STEELS

NÚRIA LLORCA-ISERN*[1], HÉCTOR LÓPEZ-LUQUE[1], ISABEL LÓPEZ-JIMÉNEZ[1], MARIA VICTORIA BIEZMA[2]

*corresponding author

Information Authors:

NÚRIA LLORCA-ISERN, CPCM Departament de Ciència dels Materials i Enginyeria Metal·lurgica, Facultat de Química, Universitat de Barcelona, Marti-Franqués 1, 08028 Barcelona, Spain, +34934021111, nullorca@ub.edu.

HÉCTOR LÓPEZ-LUQUE, CPCM Departament de Ciència dels Materials i Enginyeria Metal·lurgica, Facultat de Química, Universitat de Barcelona, Marti-Franqués 1, 08028 Barcelona, Spain, +34934021111, hlopezlu7@alumnes.ub.edu

I*SABEL LÓPEZ-JIMÉNEZ*, CPCM Departament de Ciència dels Materials i Enginyeria Metal·lurgica, Facultat de Química, Universitat de Barcelona, Marti-Franqués 1, 08028 Barcelona, Spain, +34934021111, ilopezji9@alumnes.ub.edu

MARIA VICTORIA BIEZMA Department of Earth, Materials Science and Engineering, University of Cantabria - UC, Gamazo, 1, 39004 Santander, Spain, +34942201325, maria.biezma@unican.es

ABSTRACT

The aim of this work is to find out the most suitable method for detecting and analyzing accurately the formation conditions of secondary phases, particularly Sigma-phase (σ-phase) and Chi-phase (χ-phase) in duplex stainless steels (UNS S32205 and UNS S32750). The microstructure was characterized after a solution annealing at 1080^{o}C followed by an isothermal heating at 830^{o}C for

different time ranges, ranging from 1 minute to 9 hours, in order to enlighten the controversial point concerning the mechanism of χ-phase nucleation in relation with the σ-phase. Etched samples were observed using optical microscopy (MO), and scanning electron microscopy (FESEM) with a backscattered electron detector (BSE) was used on unetched samples. Compositional microanalysis (EDS) was carried out for identifying the different phases present in the steels. Sigma phase was easily observed using different etching procedures, whereas χ-phase was only clearly detected with FESEM-BSE on unetched samples. The compositional analyses showed that the molybdenum content in χ-phase almost doubles the content of this element in σ-phase, and as a result the kinetics of nucleation and growth were also found to be remarkably faster when the alloy content in the steel is higher. In addition, chromium nitrides and carbides were also observed to precipitate as a result of the heat treatments and, in the case of the chromium nitrides, they act as a favorable site for the nucleation of σ-phase and χ-phase.

KEYWORDS

Duplex Stainless Steel, Superduplex Stainless Steel, Sigma-phase, Chi-phase, Ageing, Phase Transformations

1. INTRODUCTION

The microstructure of duplex stainless steels presents a beneficial banded mixture of austenitic (γ) and ferritic (δ) phase properties. High strength and corrosion resistance come from the ferrite, whereas the austenite phase increases ductility and resistance to uniform corrosion. Superduplex stainless steels possess a PREN (Pitting Resistance Equivalent Number) greater than 40 and therefore are extremely resistant to pitting [1, 2]. However, the exposure of these steels to high temperatures between 600^{o}C and 1000^{o}C results in the precipitation of different compounds, with σ-phase, χ-phase, chromium nitrides and carbides being the most frequently found in them [1, 3–5].

Sigma phase is a non-magnetic intermetallic based in the system of iron and chromium. It has a tetragonal crystallographic structure with 32 atoms per unit cell [6] that increases the hardness and decreases the toughness, as well as the elongation of the steel [7], and even changes the fracture type from transgranular to intergranular as the quantity of σ-phase increases [8]. Chi-phase belongs to the topologically close-packed (TCP) phases and precipitates as a ternary compound containing Fe, Cr and Mo [9] with a wide range of stoichiometry extending from the ternary χ-phase $Fe_{36}Cr_{12}Mo_{10}$ to $Fe_{36}Cr_{12}Mo_3Ti_7$ [10]. Chi-phase and σ-phase usually are found simultaneously, thus it is difficult to study their individual effect on impact properties and corrosion resistance [11].

The precipitation of these new phases causes a matrix impoverishment in alloying elements, i.e. chromium, molybdenum and niobium that leads to deterioration in toughness and corrosion resistance in the steel [1, 3, 12].

Several authors [13–15] have studied the microstructural evolution in these steels following isothermal treatments, but further information is still needed to enlighten when, where and how the formation of the secondary precipitates takes place inside these steels is necessary in order to prevent the problems related to these relevant microstructural changes.

2. MATERIAL AND METHODS

The samples used in the present study were stainless steel plates provided by Outokumpu (Finland) from duplex stainless steel grade 2205 (UNS S32205, in this study DSS 2205) and from superduplex stainless steel grade 2507 (UNS S32750, in this study SDSS 2507). The chemical composition of both stainless steels was provided by the manufacturer and is shown in Table 1.

All the samples were first solution-treated at 1080^{o}C for 30 minutes and water quenched. Subsequently, thermal annealing was conducted at 830^{o}C, followed by water quench. Temperature fluctuations did not exceed 5^{o}C in any case. The aging periods ranged from 1 minute to 9 hours. Metallographic conventional sample preparation has been carried out by grinding (P320, P600, P800 and P1200) and polishing with diamond pastes (6 μm and 1 μm).

Different etching solutions were used by previous researchers, including acid-basic and electrochemical etchings [2, 16]. The etching conditions performed in

the present study are indicated in Table 2 for acid reagents and in Table 3 for electrochemical reagents.

The microstructural analysis was conducted using an optical microscope Zeiss Axiovert 100 A, and scanning electron microscope FESEM JEOL J-7100F with a coupled Robinson BSE detector. The composition of the different phases was determined using the energy-dispersive X-ray spectroscopy system (EDS) INCA PentaFETx3. In addition, a JEOL JXA-8230 microprobe (with five WDS spectrometers) allowed us to obtain a higher chemical composition accuracy.

3. RESULTS AND DISCUSSION

Both optical microscope and FESEM observation of the etched samples were performed in order to analyze the microstructural changes occurred in the annealed DSS 2205 and SDSS 2507 samples for the different thermal treatment lengths.

3.1 Optical microscopy characterization

Satisfactory results were obtained with some of the etching reagents referred in the literature, but others were not considered satisfactory and therefore were rejected for optical microscope and FESEM characterization (Table 3).

Glyceregia reagent (Fig. 1a and 1b) provides the best contrast between ferrite phase and σ-phase when the latter occupies a low percentage in the microstructure, but the etching time step, close to 2 minutes, could be considered too high in particular cases if a significant number of samples have to be observed. It is worth mentioning that this reagent is the only one in which σ-phase is observed as a white phase in the optical microscope. Grosbeck's reagent (Fig. 1c and 1d) has the advantage of differentiating nitrides (darkest phase), but requires an imprecise time of etching (1-10 minutes). Between the different chemical etching reagents, Murakami reagent (Fig. 1e and 1f) was found to be the most convenient due to its short time of etching needed and sufficient contrast between the different phases. However, it is difficult to identify ferrite phase when present in small quantities. If an electrochemical etching has to be employed, the 20% NaOH solution (Fig. 1g and 1h) provided good results as long as the operation conditions are appropriately controlled, and also it is a fast etching, easy to prepare and it does not produce any toxicity problem, but again distinguishing between ferrite phase and σ-phase when the amount of σ-phase outnumbers the amount of ferrite phase becomes complicated.

The specific microstructure, the time of etching and the sensitivity to the reagents concentration are important to achieve a good identification of the phases hence there is not a general ideal reagent for duplex and superduplex stainless steels. Examples of this fact can be observed when χ-phase or carbides are known to be present in the microstructure but could not be seen in optical microscopy of etched samples, due to the detachment from the matrix or to their small size.

3.2 Scanning electron microscopy characterization.

The samples were also characterized by FESEM, firstly on etched samples since previous studies used this procedure [2, 15]. Unfortunately, the results were unsatisfactory due to the formation of oxide layers which complicated the compositional analysis. Also, certain phase boundaries are initially dissolved as can be seen in Figure 2; if any phase is formed close to or in this interphase it may be lost by etching. Therefore, unetched samples were imaged in the FESEM and a back-scattered electron detector was used due to its ability to differentiate between phases according to their mean atomic number without need of chemical etching. Since σ-phase and specially χ-phase contain a higher percentage of molybdenum, a heavier element than the other present in these steels, the greyscale contrast of these phases should be significant compared to that of ferrite and austenite (Fig. 3). In Figure 3, the different phases can be clearly identified as ferrite (darkest phase), austenite (dark grey), σ-phase (light grey) χ-phase (brighter phase), and some dark spots which can be observed at the interphase between ferrite and austenite and will be studied further on.

Energy-dispersive X-ray spectroscopy (EDS) was used in order to identify from compositional information the different microstructural phases and compounds in the samples. The results obtained for DSS 2205 and SDSS 2507 are shown in Table 4. Initially only two phases are present in the microstructure: Austenite, which contains a higher relative percentage of nickel (gammagen element) and ferrite, which is richer in chromium (alphagen element). The intermetallic

phases started to nucleate after the samples were heat treated between 1 and 5 minutes: σ-phase, with a high content in chromium and molybdenum, and χ-phase, which shows a remarkably higher content in molybdenum than any other phase present and a similar content in chromium to that of ferrite phase.

The first microstructural change was related to the precipitation of small dark grey and black spots in samples annealed during shorter times than 3 minutes (Fig. 4).

Wavelength-dispersive spectroscopy (WDS) was performed in order to confirm the nature of these precipitates. An accumulation of nitrogen and chromium in the dark gray particles confirmed they are chromium nitrides (Fig. 5). These chromium nitrides nucleated at ferrite/ferrite and austenite/ferrite boundaries, and at ferrite/ferrite/ferrite triple points. This precipitation is favored by a high cooling rate as a result of accommodating substantial amounts of nitrogen in ferrite supersaturated solid solution, as previously reported by Nilsson and Wilson [1].

On the other hand, the other dark phase distributed mainly intragranularly and heterogeneously as dark spots in all the phases in the form of globular particles, the absence of nitrogen and a concentration in carbon indicated they are carbides. None of the WDS locations showing high nitrogen content are high carbon content coincident, which decreases any potential for carbonitrides presence (Fig. 6).

3.3 Phase analysis in duplex and superduplex stainless steel

Both σ-phase and χ-phase start their nucleation process soon after the initial ageing treatment and after the precipitation of nitrides and carbides (between 3 and 5 minutes for DSS 2205 and between 1 and 3 minutes for SDSS 2507) as can be observed in Figure 7. As previously reported [17], the addition of a strong ferrite stabilizer into the stainless steels (Cr, Si or Mo) rapidly leads to the formation of the intermetallic phases. Sigma-phase and χ-phase have a combined growth, although the amount of χ-phase is certainly higher at the beginning of the process, the main reason being the apparent inability of σ-phase to nucleate at ferrite/ferrite boundaries without a previously precipitated χ-phase at the same site. A probable reason for this phenomenon could be the ferrite stabilizers diffusion values at low time treatments, which might cause a higher local supersaturation that favors χ-phase nucleation, instead of the nucleation of σ-phase. On the other hand, our results show that both phases were found at ferrite/ferrite/austenite triple points and ferrite/austenite boundaries at these stages, nucleating at the phase boundary in the highly chromium concentrated region of ferrite with a hemispheric morphology, which were observed to only grow towards ferrite phase.

Chromium nitrides, which precipitate before σ-phase and χ-phase, act as a favorable site for the nucleation of the new intermetallic phases (Fig. 8). However, their position was invariable after their precipitation and they remain at the same location even after the grain boundaries are displaced as a result of the formation of secondary austenite (Fig. 9). As reported by Breda et al. [18],

the long-time treated samples showed a less interconnected distribution of nitrides as a result of the growth of σ-phase and χ-phase.

However, at longer annealing time σ-phase grows following the mechanism described by Nilsson and Wilson [1]. Further precipitation and growth of σ-phase occurs and simultaneously χ-phase transforms to σ-phase. This phase transformation happens also to the χ-phase located at ferrite/ferrite interfaces (Fig. 10). After 9 hours at 830^{o}C, in SDSS 2507 σ-phase has almost completely substituted the ferrite phase and χ-phase cannot be longer detected (Fig. 11a). On the contrary, this process is slowed in DSS 2205 and ferrite and χ-phase still remain in significant percentages after 9 hours of heat treatment (Fig. 11b). Final σ-phase shape is somehow blunted compared to the starting ferrite morphology, caused by the linking between single sigma crystals. Consequently, austenite phase shows an enlargement if it is compared with the morphology and dimensions of the specimens without thermal treatment. Using a direct observation of early stages of the process in both stainless steels (Fig. 7) compared to longer heat treated samples (Fig. 11), a displacement of the ferrite/austenite boundary towards the ferrite grain is observed.

Simultaneously to the enrichment in chromium and molybdenum of σ-phase and χ-phase during their propagation process, nickel diffuses into ferrite. The enrichment of austenite stabilizing elements in ferrite and the loss of ferrite stabilizing elements, leads to an unstable ferrite that transforms into secondary austenite [13]. The variation of chromium and molybdenum in the four different observed phases (δ, γ, σ and χ) related to DSS 2205 is shown in Figure 12, and to SDSS 2507 in Figure 13. In the case of this steel, although a fluctuation in

chromium content can be observed in ferrite between different samples, it cannot be directly related to the diffusion towards the nucleated phases since the variations are too small, probably because this phenomenon takes place at the boundaries and the analyses were carried out in interior points of the ferrite grains. Concerning the variations in molybdenum, an element in lower percentage than chromium, a substantial compositional decrease was observed in ferrite phase for long annealing times attributed to the diffusion of this element towards the formation of σ-phase (grey lines), and especially towards the formation of χ-phase.

In the case of SDSS, chromium content in ferrite starts to diminish after only 30 minutes and at 9 hours a 20% of Cr has moved towards the newly formed intermetallics. Regarding molybdenum, the variation is more remarkable showing a loss of 60% from the initial ferrite after 9 hours of treatment. The main reason for these changes being more noticeable in SDSS can be attributed to the faster kinetics of nucleation and growth of σ-phase and χ-phase compared to the kinetics in DSS, especially due to the higher Mo content in the SDSS, which controls the diffusion kinetics and contributes to the increase in the driving force of the genesis of the intermetallic compounds [18]. Therefore, the ferritic phase associated dimension is smaller and also smaller is the diffusion path consequently, and any point is sufficiently close to the grain boundary to be subjected to high diffusion rates.

ED-Linescan microanalyses were performed in order to obtain a proper tool to understand the relationship between composition and microstructure. A

linescan microanalysis in DSS treated for 1 hour is shown in Figure 14, which confirms the above presented hypothesis: nickel gathers in austenite and iron content diminishes in the intermetallic phases, while chromium and molybdenum presence increase considerably in σ-phase and χ-phase respectively, although a lower but remarkable peak can also be noticed in σ-phase for molybdenum. Chromium or molybdenum depletion zones have not been detected in this study as other authors have previously reported [13, 19]. The reason for this can be the width of the depletion zones, which are too small to be detected by EDS, or because the diffusion is enhanced and compensates and homogenizes these elements in ferrite and austenite.

During the eutectoid transformation of ferrite into σ-phase and χ-phase, ferrite is destabilized due to chromium loss and hence can transform into secondary austenite and σ-phase according to the following reaction [20]:

$$\delta \rightarrow \sigma + \gamma_2$$

In Figure 15 this multiple transformation and the coexistence of phases with different composition contrast in the form of granulated ferrite grains can be observed. The lighter grey can be assigned to the newly formed secondary austenite. Another hypothesis to explain the different contrast clearly visible at higher resolution can be the nucleation of nanometric σ-phase crystals encouraged by the high content in chromium and molybdenum present in ferrite phase; their growth is not thermodynamically favored due to the low diffusion rates inside the ferrite grains hindering further grow.

As previously described, all these “new” phases that nucleated in both duplex steels appeared at very short durations of heat treatment, and except the carbides, they all precipitated at grain boundaries, which suggests it is advisable to avoid employing these steels at this temperature range since the mechanical properties linked with them will be altered if the evolution of the microstructure occurs as has been mentioned [8, 21]. However, the mechanical properties of a duplex stainless steel formed only by austenite and σ-phase at similar percentages are yet to be thoroughly investigated, but it is possible that after the transformations have occurred, the mechanical behavior could be better compared with a steel in which there are still remains of ferrite, and even useful for some determined applications.

4. CONCLUSIONS

The microstructural changes in duplex stainless steel UNS S32205 and the superduplex stainless steel UNS S32750 at different thermal treatments have been investigated. Different chemical etchings for characterizing the microstructure were evaluated. Due to the alterations caused in the morphology, the integrity and the chemical composition of the phases, FESEM-BSE on unetched samples was found to be the recommended method to study these steels and clearly identify the different phases without using crystallographic analysis

Various phases began to precipitate at shorter time, less than 5 minutes in both duplex and superduplex steels: chromium nitrides and carbides, χ-phase (phase with the highest content in molybdenum) and finally σ-phase, ranking in this order. Chromium nitrides act as a favorable site for the nucleation of χ-phase, and both of them then encourage the formation of σ-phase. However, the growth of the chromium nitrides and χ-phase slows down earlier than the growth of σ-phase itself. Sigma-phase completely consumes χ-phase at longer heat treatments, whereas the chromium nitrides remain stable through time and their location is kept from their original nucleation site.

During the nucleation of these new intermetallic phases, chromium and molybdenum diffuse from the ferritic phase and ferrite transforms into secondary austenite as a result of losing these alphagen elements. In the superduplex stainless steel for example, the content of chromium in ferrite decreases 27% after 9 hours of heat treatment and the content in molybdenum falls down 66%.

The kinetics of the transformations occurring in duplex steels were found to be faster when the percentage in alloying elements was higher, specifically the content in chromium and molybdenum. In the superduplex stainless steel UNS S32750, after 9 hours of treatment the σ-phase almost completely replaces ferrite phase, while after the same time in the duplex stainless steel UNS S32205 the ferritic phase still remains with relevant percentages. As a result of the formation of σ-phase and secondary austenite, the boundaries between the different phases are blurred, losing the originally banded morphology.

ACKNOWLEDGEMENTS

The authors would like to thank Outokumpu (www.outokumpu.com) for providing the material, and the CCiTUB for their technical support.

REFERENCES

[1] J. O. Nilsson and A. Wilson, “Influence of isothermal phase transformations on toughness and pitting corrosion of super duplex stainless steel SAF 2507,” *Materials Science and Technology*, vol. 9, no. 7, pp. 545–554, Jul. 1993.

[2] J. Michalska and M. Sozańska, “Qualitative and quantitative analysis of σ and χ phases in 2205 duplex stainless steel,” *Materials Characterization*, vol. 56, no. 4–5, pp. 355–362, Jun. 2006.

[3] S. Bernhardsson, “The corrosion resistance of duplex stainless steels,” *Duplex Stainless Steels’91,* vol. 1, pp. 185–210, 1991.

[4] T. H. Chen, K. L. Weng, and J. R. Yang, “The effect of high-temperature exposure on the microstructural stability and toughness property in a 2205 duplex stainless steel,” *Materials Science and Engineering: A*, vol. 338, no. 1–2, pp. 259–270, Dec. 2002.

[5] H. Sieurin and R. Sandström, “Sigma phase precipitation in duplex stainless steel 2205,” *Materials Science and Engineering: A*, vol. 444, no. 1–2,

pp. 271–276, Jan. 2007.

[6] S. Atamert and J. E. King, “Sigma-phase formation and its prevention in duplex stainless steels,” *J Mater Sci Lett*, vol. 12, no. 14, pp. 1144–1147, Jan. 1993.

[7] I. K. JooSuk LEE, “Application of Small Punch Test to Evaluate Sigma-Phase Embrittlement of Pressure Vessel Cladding Material,” *Journal of Nuclear Science and Technology*, vol. 40, pp. 664–671, 2003.

[8] M. V. Biezma, C. Berlanga, and G. Argandona, “Relationship between microstructure and fracture types in a UNS S32205 duplex stainless steel,” *Materials Research*, vol. 16, no. 5, pp. 965–969, Oct. 2013.

[9] Y. H. Lee, K. T. Kim, Y. D. Lee, and K. Y. Kim, “Effects of W substitution on ς and χ phase precipitation and toughness in duplex stainless steels,” *Mater. Sci. Technol.*, vol. 14, no. 8, pp. 757–764, Aug. 1998.

[10] I. C. I. Okafor and O. N. Carlson, “Equilibrium studies on a chi phase-strengthened ferritic alloy,” *MTA*, vol. 9, no. 11, pp. 1651–1657, Nov. 1978.

[11] R. Gunn, *Duplex stainless steels: microstructure, properties and applications*. Elsevier, 1997.

[12] A. F. Padilha, C. F. Tavares, and M. A. Martorano, “Delta Ferrite Formation in Austenitic Stainless Steel Castings,” *Materials Science Forum*, vol. 730–732, pp. 733–738, Nov. 2012.

[13] O. S. Michael Pohl, “Effect of intermetallic precipitations on the properties of duplex stainless steel,” *Materials Characterization*, no. 1, pp. 65–71, 2007.

[14] S. K. Ghosh and S. Mondal, “High temperature ageing behaviour of a duplex stainless steel,” *Materials Characterization*, vol. 59, no. 12, pp. 1776–1783, Dec. 2008.

[15] D. M. Escriba, E. Materna-Morris, R. L. Plaut, and A. F. Padilha, “Chi-phase precipitation in a duplex stainless steel,” *Materials Characterization*, vol. 60, no. 11, pp. 1214–1219, Nov. 2009.

[16] G. F. V. Voort, *Metallography, Principles and Practice*. ASM International, 1984.

[17] C.-C. Hsieh and W. Wu, “Overview of Intermetallic Sigma Phase Precipitation in Stainless Steels,” *ISRN Metallurgy*, vol. 2012, pp. 1–16, 2012.

[18] M. Breda, M. Pellizzari, and M. Frigo, “σ-Phase in Lean Duplex Stainless Steel Sheets,” *Acta Metall. Sin. (Engl. Lett.)*, vol. 28, no. 3, pp. 331–337, Jan. 2015.

[19] K. H. Lo, C. T. Kwok, and W. K. Chan, “Characterisation of duplex stainless steel subjected to long-term annealing in the sigma phase formation temperature range by the DLEPR test,” *Corrosion Science*, vol. 53, no. 11, pp. 3697–3703, Nov. 2011.

[20] K. M. Lee, H. S. Cho, and D. C. Choi, “Effect of isothermal treatment of SAF 2205 duplex stainless steel on migration of δ/γ interface boundary and growth of austenite,” *Journal of Alloys and Compounds*, vol. 285, no. 1–2, pp. 156–161, Jun. 1999.

[21] S. Topolska and J. Labanowski, “Effect of microstructure on impact toughness of duplex and superduplex stainless steels,” *Journal of Achievements in Materials and Manufacturing Engineering*, vol. 36, no. 2, pp. 142–149, 2009.

Table 1. Chemical composition of DSS 2205 and SDSS 2507 (%wt, balance Fe).

	C	Si	Mn	P	S	Cr	Ni	Mo	N	Cu	Ce
2205	0.015	0.40	1.5	0.018	0.001	22.49	5.77	3.21	0.184	0.18	0.002
2507	0.018	0.26	0.84	0.019	0.001	25.08	6.88	3.82	0.294	0.17	-

Table 2. Acid and electrochemical reagents and etching conditions used to reveal the microstructure of DSS and SDSS [2, 16].

Chemical reagent	Etching conditions
Glyceregia	Time of etching: 2 min Temperature: 20ºC
Grosbeck's	Time of etching : 1-10 min Temperature: 60-90ºC
Marble's	Time of etching : 3-10 s Temperature: 20ºC
Murakami's (modified)*	Time of etching : 3-5 s Temperature: 20ºC
Villela's	Time of etching : 1 min Temperature: 20ºC
Electrochemical NaOH	Time of etching : 10s Potential: 3 V Cathode: Pt
Electrochemical HCl/Etanol	Time of etching : 3-5s Potential: 1.5V Cathode: Pt

* KOH was replaced by NaOH.

Table 3. Summary of the ability to reveal the microstructure in optical microscopy for the different etching reagents used.

Etching	Current study observation
Glyceregia	Grain boundaries and σ-phase
Grosbeck's	Selective etching for σ-phase and nitrides
Marble's	Unsatisfactory performance obtained
Murakami's (modified)	Reveals ferrite and σ-phase
Villela's	Unsatisfactory performance obtained
Electrochemical NaOH	Reveals ferrite and σ-phase, nitrides are visible but not completely revealed
Electrochemical HCl/Etanol	Unsatisfactory performance obtained

Table 4. Evolution of phases obtained after heat treatment with chemical composition (%wt) for DSS 2205 and SDSS 2507.

Annealing time	Composition								
	Phase	DSS 2205				SDSS 2507			
		Element (%wt)							
		Cr	Fe	Ni	Mo	Cr	Fe	Ni	Mo
-	Austenite (γ)	21.6	67.4	6.5	2.6	24.9	62.6	8.3	3.3
	Ferrite(δ)	24.9	64.6	4.4	4.6	27.3	60.9	5.9	5.2
10 min	Austenite (γ)	21.4	67.6	7.0	2.1	23.6	62.5	8.5	3.9
	Ferrite (δ)	25.2	65.3	4.1	4.4	26.6	65.8	3.7	3.1
	Sigma (σ)	28.3	57.7	3.8	8.2	30.3	56.7	3.7	8.2
	Chi (χ)	23.3	57.7	3.2	14.2	26.1	54.1	4.3	14.9
300 min	Austenite (γ)	21.1	65.9	6.3	2.4	24.5	62.8	8.9	3.0
	Ferrite (δ)	23.3	67.8	2.7	1.6	21.7	68.9	6.3	1.4
	Sigma (σ)	30.1	56.8	2.5	8.9	30.7	56.2	4.0	7.6
	Chi (χ)	26.9	53.8	2.5	16.3	29.8	53.4	3.7	14.0
540 min	Austenite (γ)	21.7	64.0	7.2	2.7	24.2	60.2	8.0	3.2
	Ferrite (δ)	24.7	69.0	2.1	2.0	20.1	67.9	6.1	2.0
	Sigma (σ)	29.6	59.0	1.8	6.1	31.2	54.2	3.2	8.5
	Chi (χ)	25.1	56.0	2.3	16.5	-	-	-	-

FIGURES CAPTION

Figure 1. Microstructural study on DSS (left) and SDSS (right) treated for 1 hour at 830^{o}C. Micrographs A) and B) correspond to Glyceregia reagent etching, C) and D) to Grosbeck's reagent etching, E) and F) to Murakami (modified) reagent etching and G) and H) to electrochemical 20% NaOH etching.

Figure 2. FESEM-BSE image of DSS 2205 aged 1 hour at 830^{o}C etched with NaOH, showing austenite (light grey), ferrite (dark grey) and oxide layers (white) above σ-phase.

Figure 3. FESEM-BSE image of DSS 2205 aged 1 hour at 830^{o} in which ferrite (darkest phase), austenite (dark grey), σ-phase (light grey) and specially χ-phase (brighter phase) can be clearly seen.

Figure 4. FESEM-BSE image of DSS 2205 treated for 3 minutes. Chromium nitrides are located at the ferrite/austenite and the ferrite/ferrite boundaries (solid circles). Carbides are identified all over the austenite and ferrite phases as small black spots (group of carbides in both phases marked with dotted circles).

Figure 5. WDS of SDSS 2507 treated for 3 minutes at 830^{o}C. A) SEM-BSE image showing the dark chromium nitrides encircled. B) Chromium accumulations. C) Nitrogen accumulations.

Figure 6. WDS of SDSS 2507 treated for 3 minutes at 830^{o}C. A) SEM-BSE image showing some of the dark carbides encircled. B) Carbon accumulations. C) Nitrogen accumulations.

Figure 7. FESEM-BSE image of A) DSS 2205 treated at 830^{o}C during 5 minutes and B) SDSS 2507 treated at 830^{o}C during 4 minutes.

Figure 8. Chromium nitrides in A) DSS treated for 5 minutes at 830^{o}C, located at ferrite/ferrite and ferrite/austenite boundaries, acting as nucleation sites for χ-phase, and in B) SDSS treated for 3 minutes at 830^{o}C, precipitating at ferrite/austenite

boundaries and at triple ferrite/ferrite/ferrite points, acting as a site of nucleation for σ and χ phases.

Figure 9. Chromium nitrides in DSS treated at 830°C for 9 hours showing a displacement from their original position at grain boundaries and a less interconnected formation.

Figure 10. FESEM-BSE image of A) DSS 2205 treated for 20 minutes and B) SDSS 2507 treated for 10 minutes, both at 830°C.

Figure 11. FESEM-BSE image of A) DSS treated for 9 hours and B) SDSS 2507 treated for 9 hours, both at 830°C.

Figure 12. Chromium and molybdenum variations in ferrite (blue lines), austenite (orange lines), σ-phase (grey lines) and χ-phase (yellow lines) in DSS 2205.

Figure 13. Chromium and molybdenum variations in ferrite (blue lines), austenite (orange lines), σ-phase (grey lines) and χ-phase (yellow lines) in SDSS 2507.

Figure 14. A) FESEM-BSE linescan microanalysis of DSS 2205 treated at 830°C for 1 hour. Distribution of B) iron, C) chromium, D) nickel and E) molybdenum.

Figure 15. FESEM-BSE image of SDSS 2507 treated at 830°C for 1 minute, ferrite phase transforming into σ-phase, χ-phase and secondary austenite.

High-resolution Figure(s)
Click here to download high resolution image

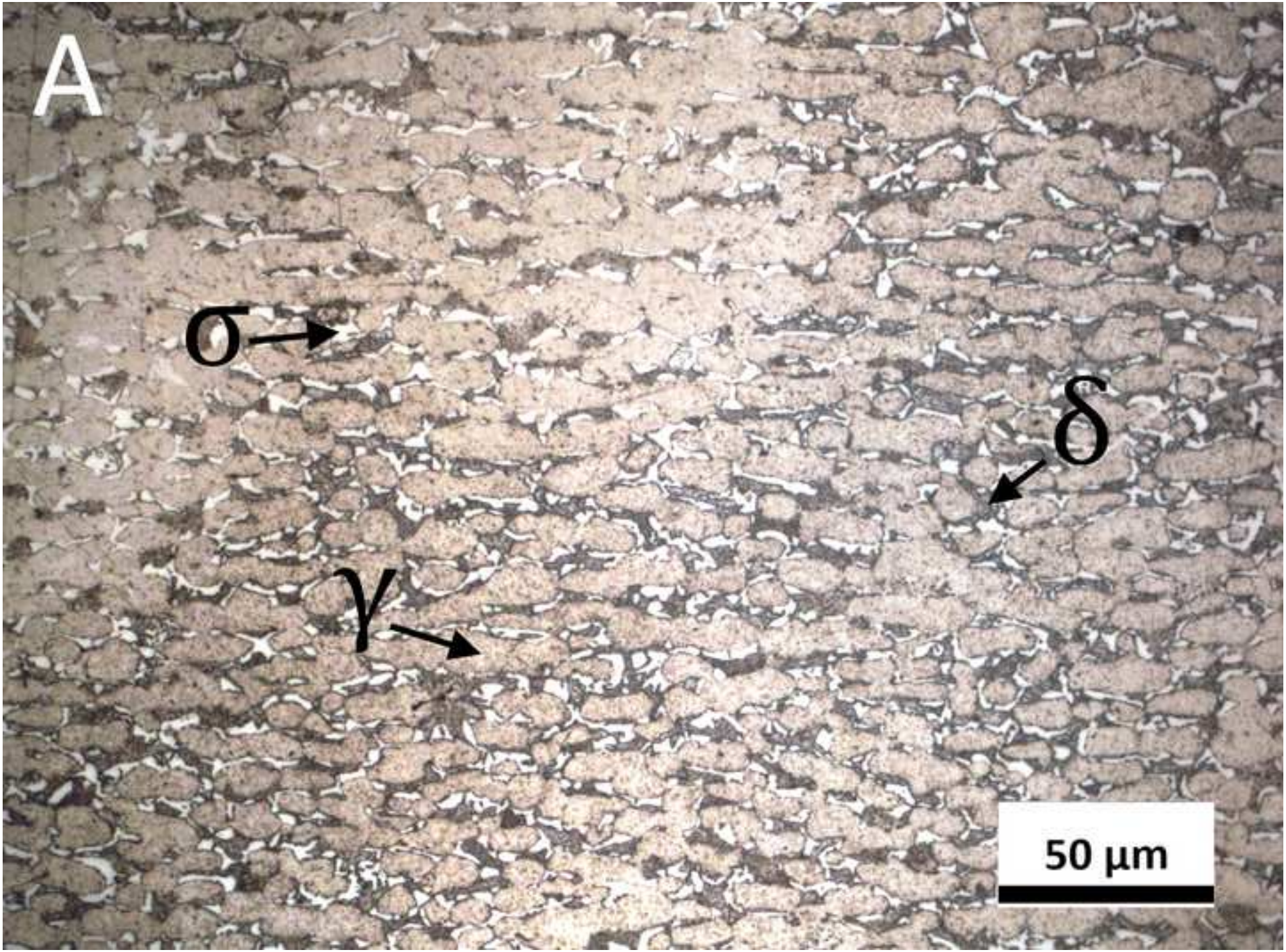

High-resolution Figure(s)
Click here to download high resolution image

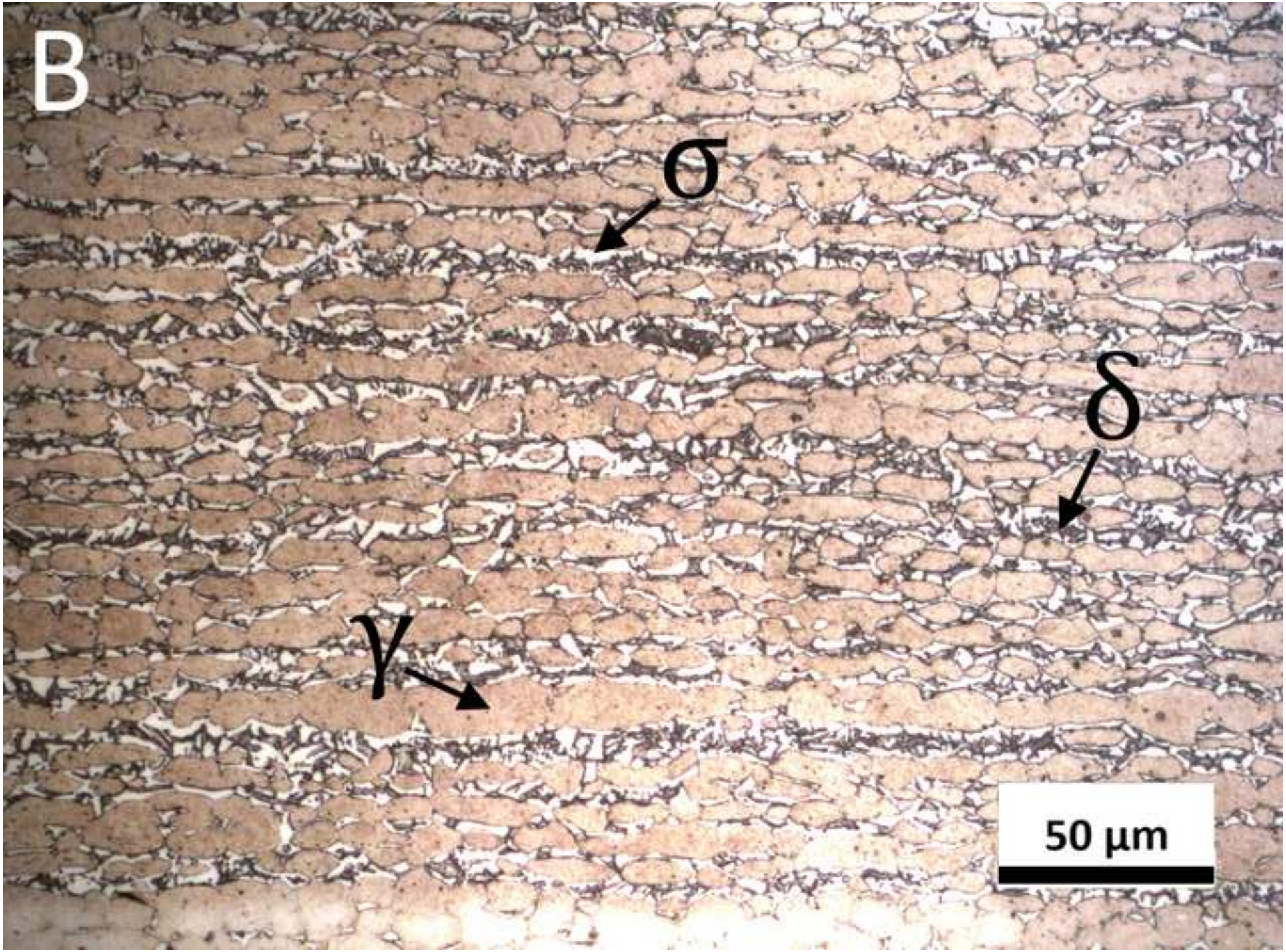

High-resolution Figure(s)
Click here to download high resolution image

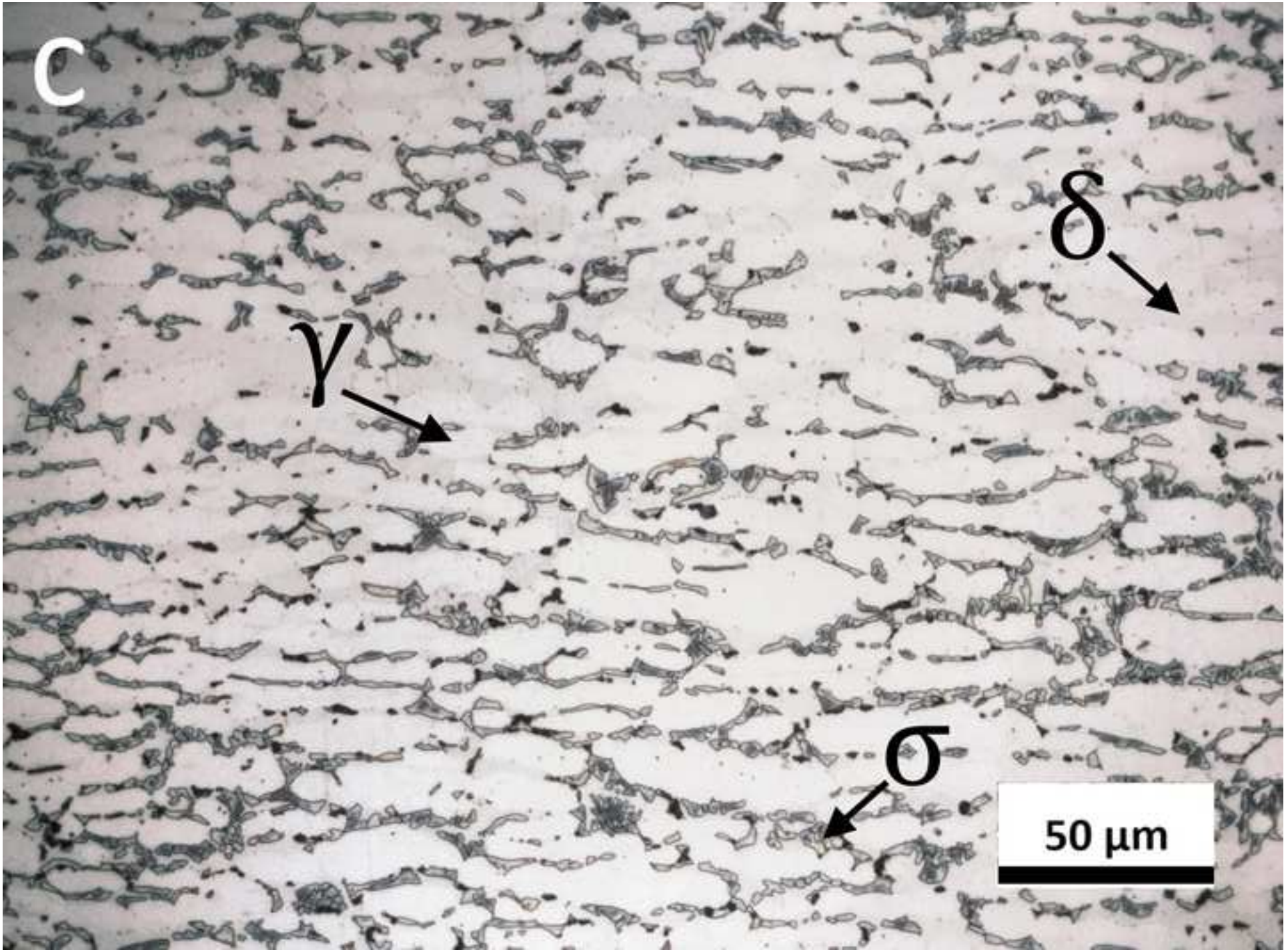

High-resolution Figure(s)
Click here to download high resolution image

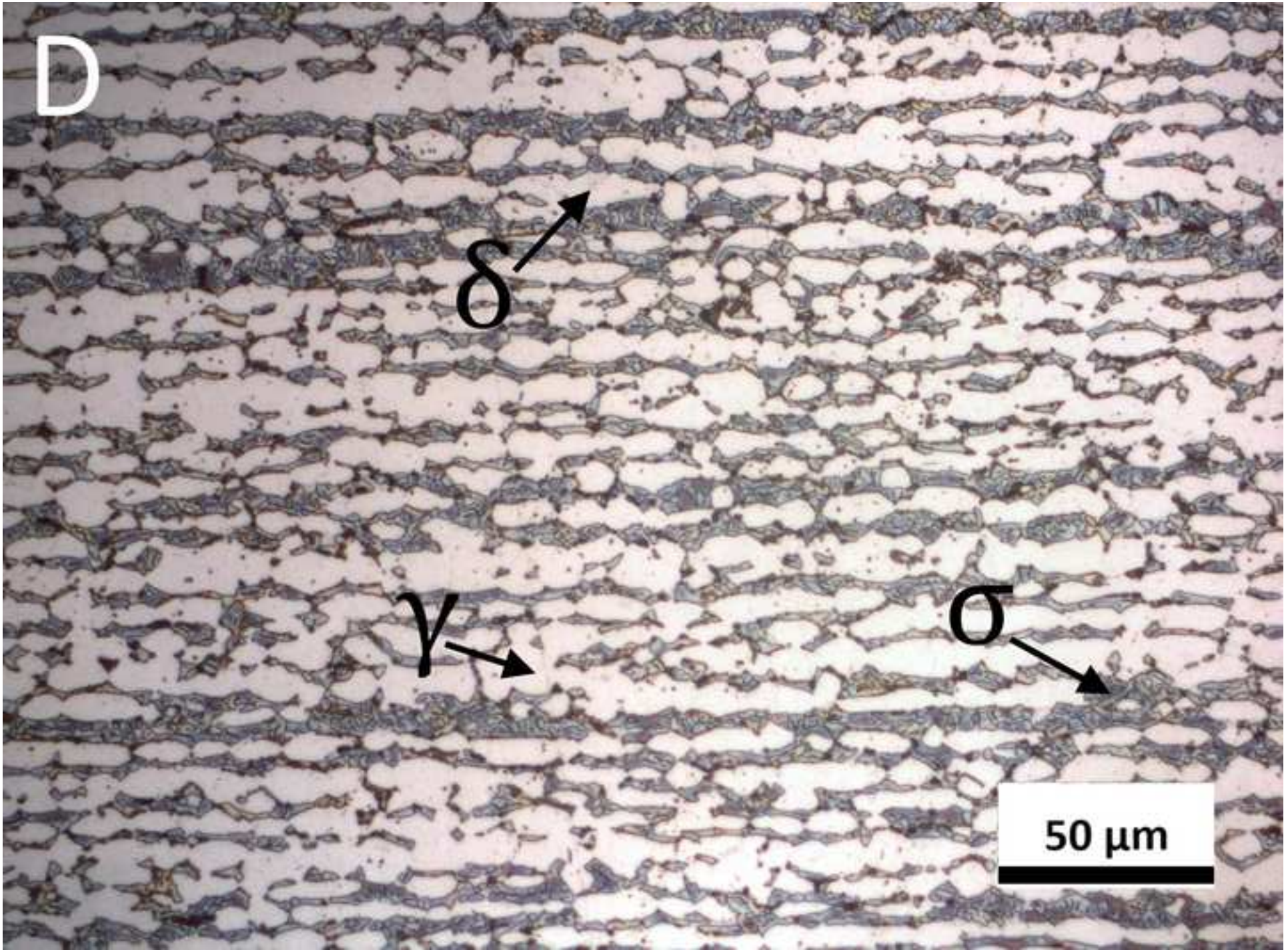

High-resolution Figure(s)
Click here to download high resolution image

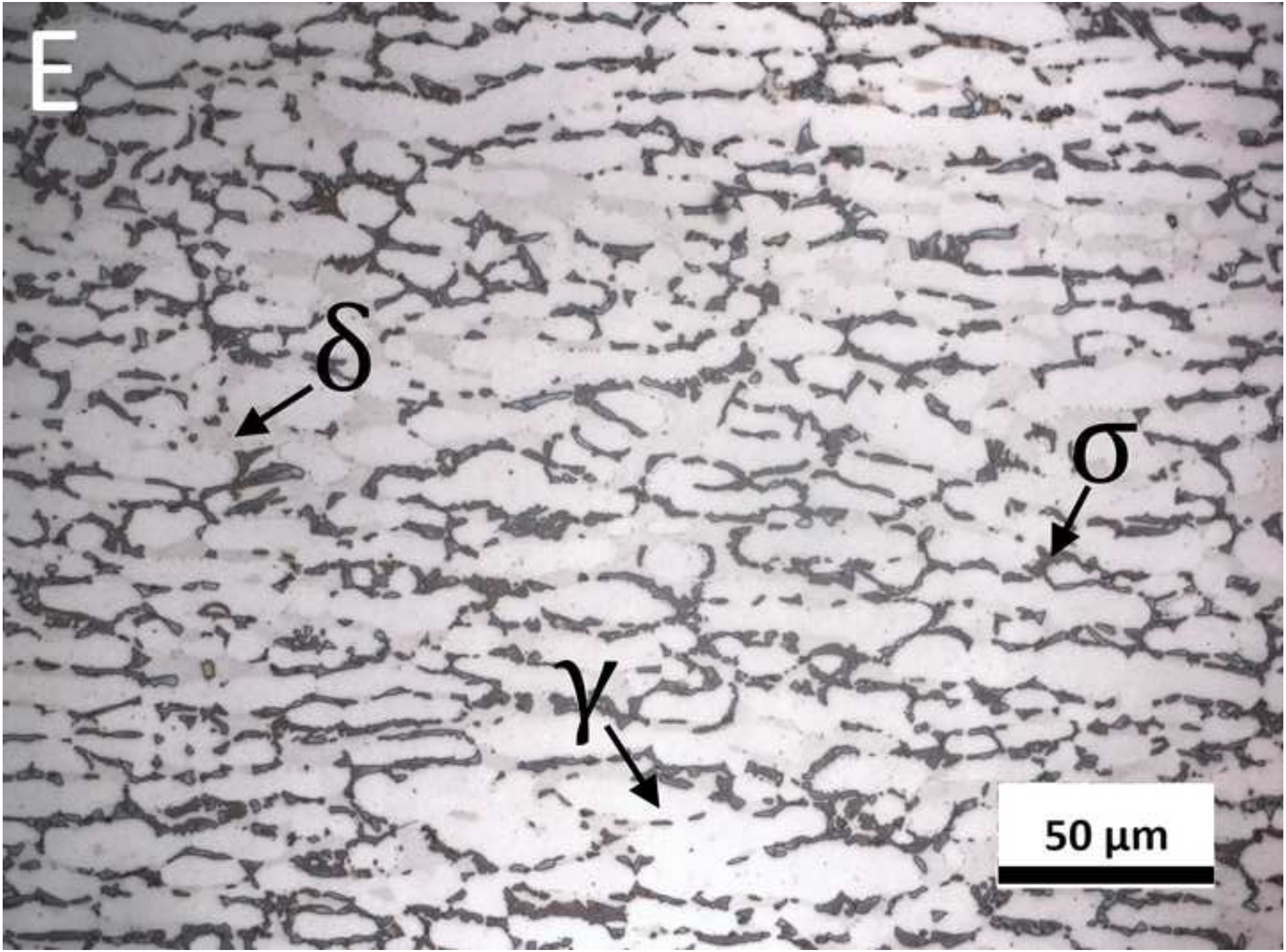

High-resolution Figure(s)
Click here to download high resolution image

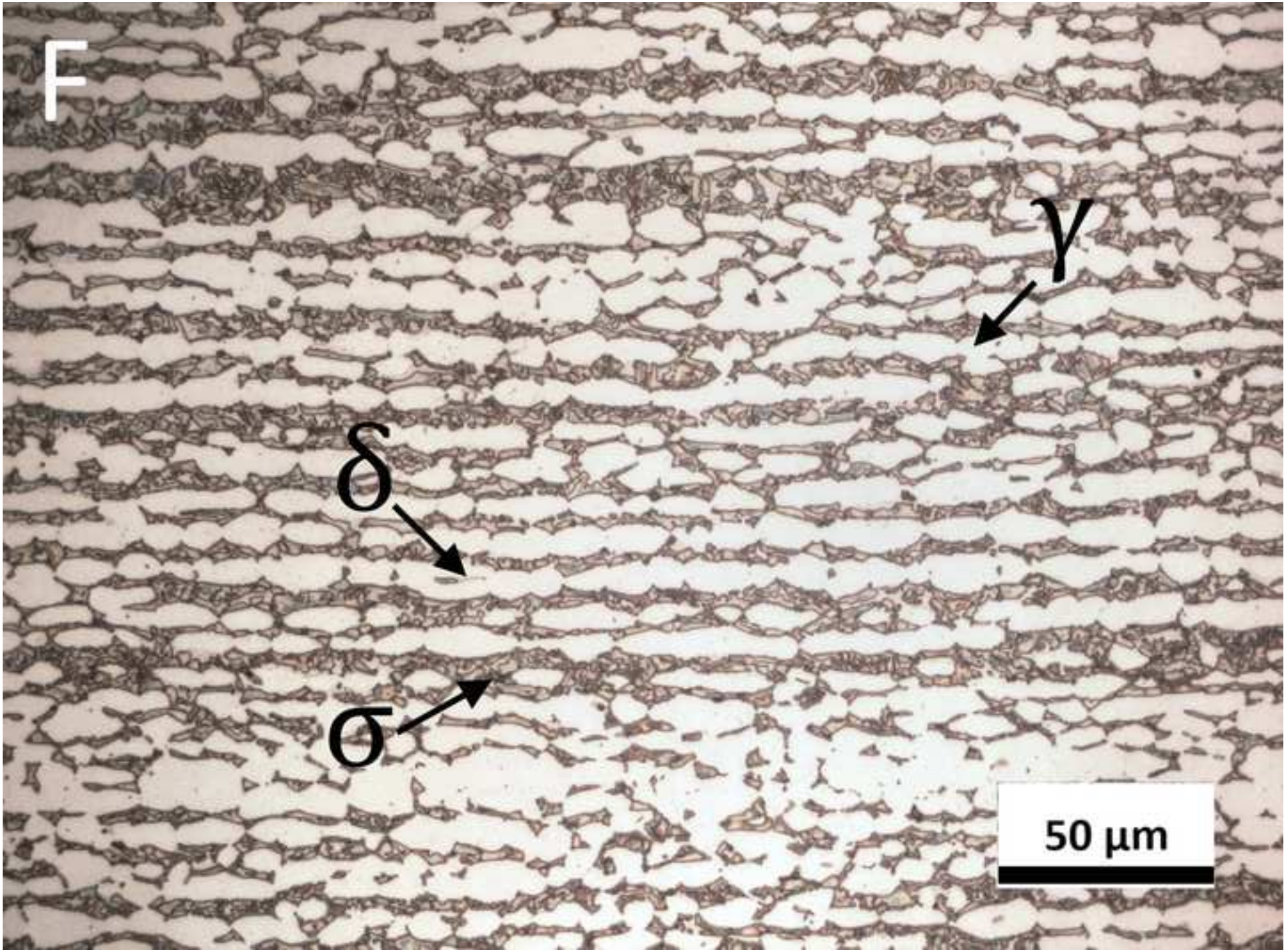

High-resolution Figure(s)
Click here to download high resolution image

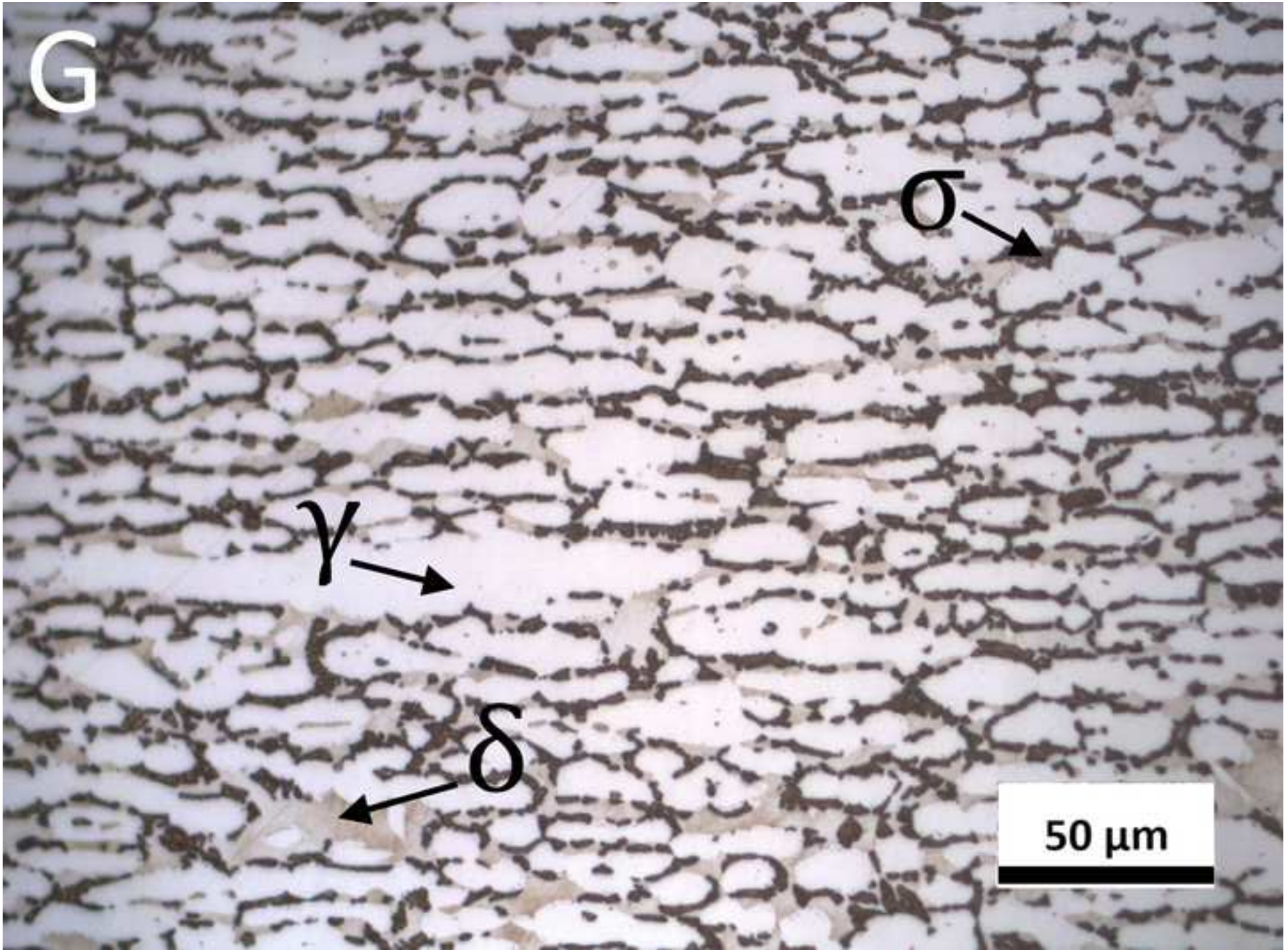

High-resolution Figure(s)
Click here to download high resolution image

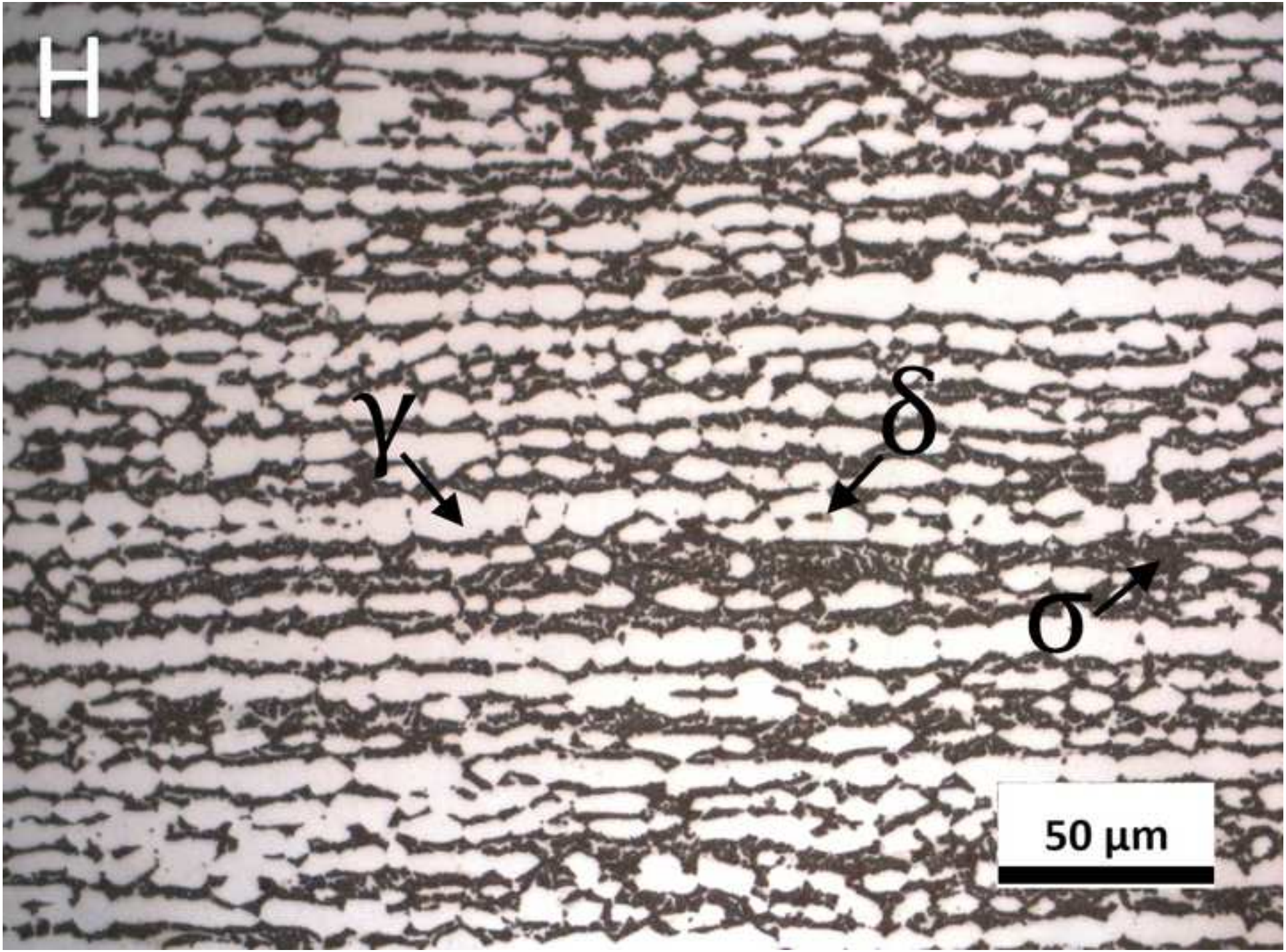

High-resolution Figure(s)
Click here to download high resolution image

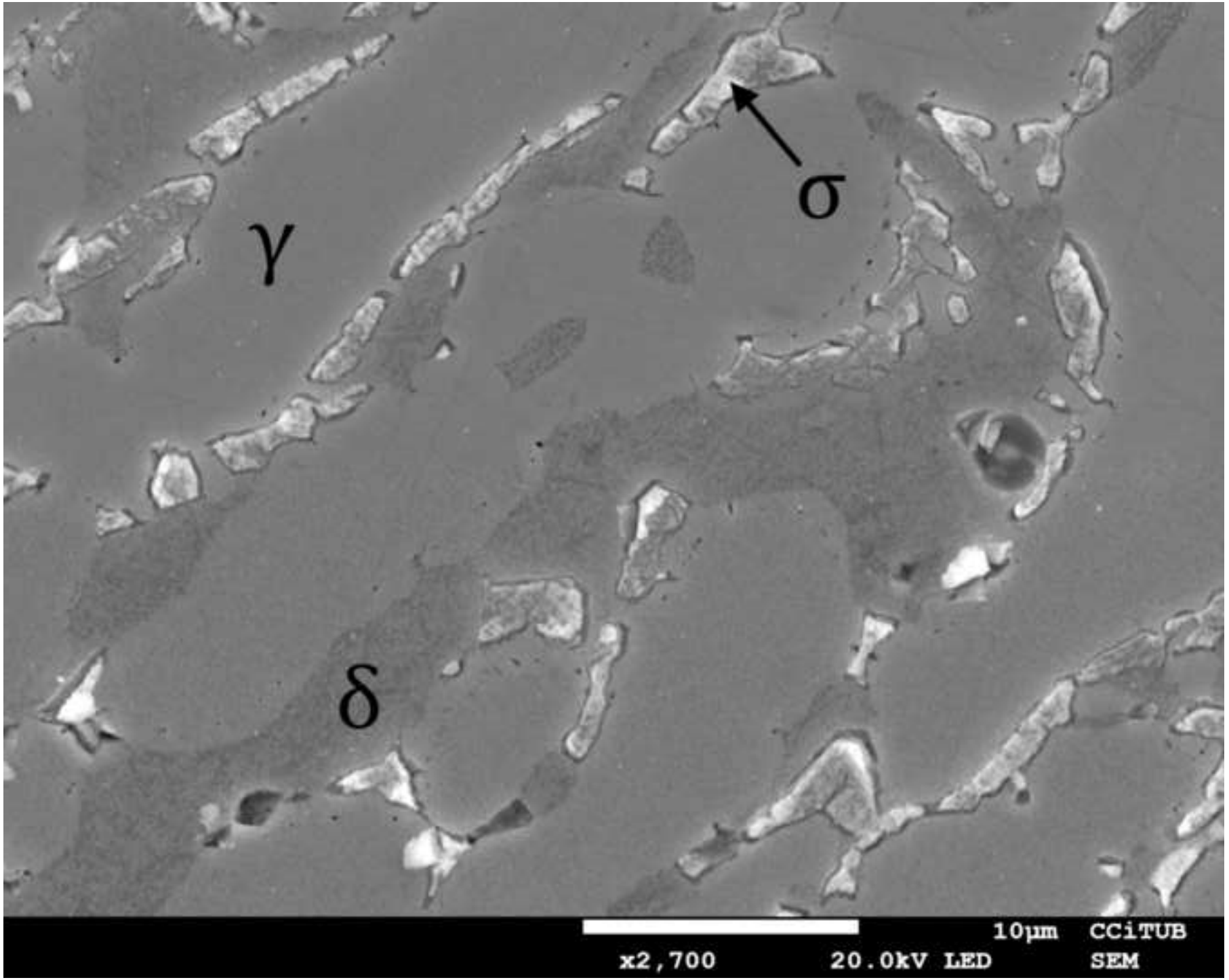

High-resolution Figure(s)
Click here to download high resolution image

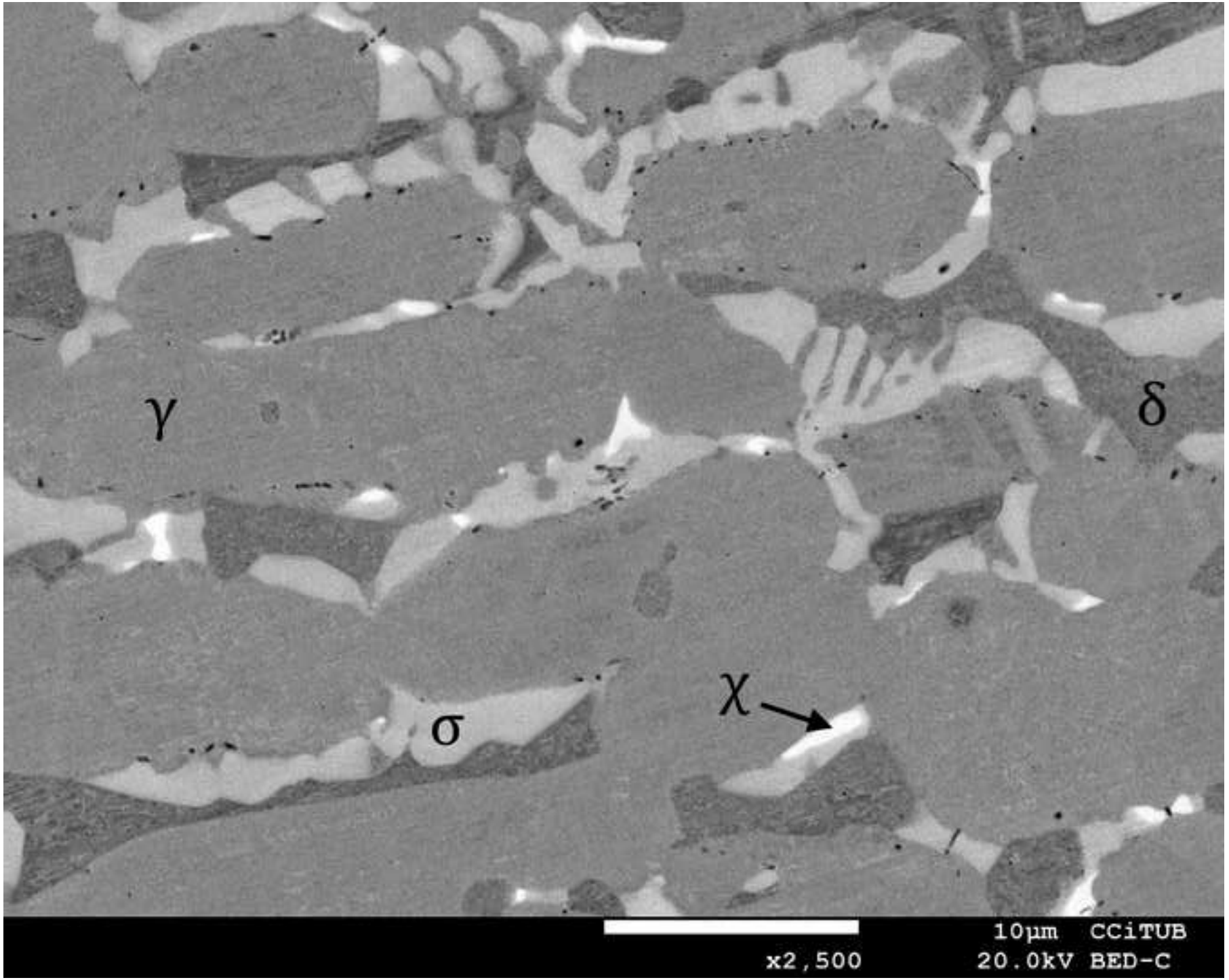

High-resolution Figure(s)
Click here to download high resolution image

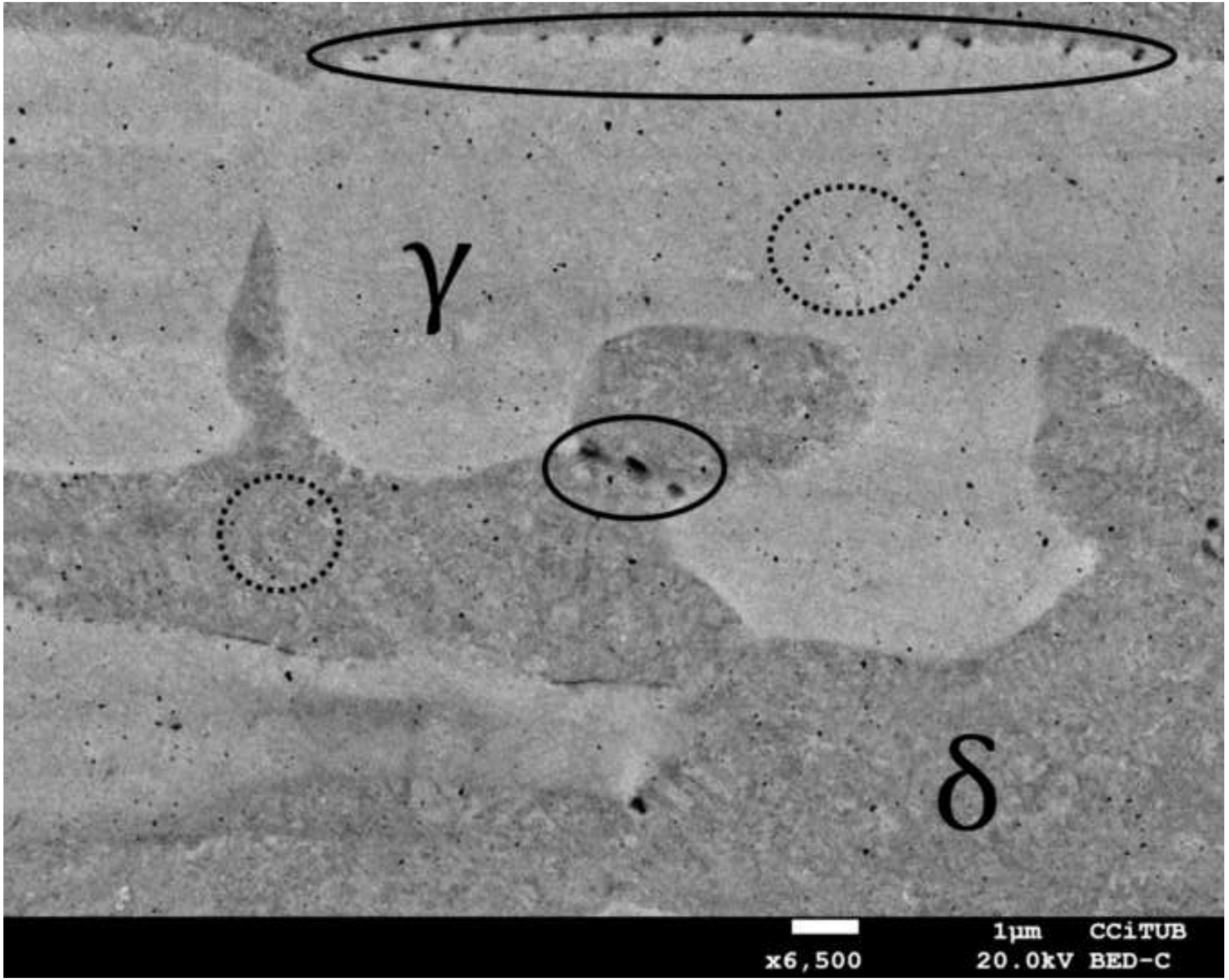

High-resolution Figure(s)
Click here to download high resolution image

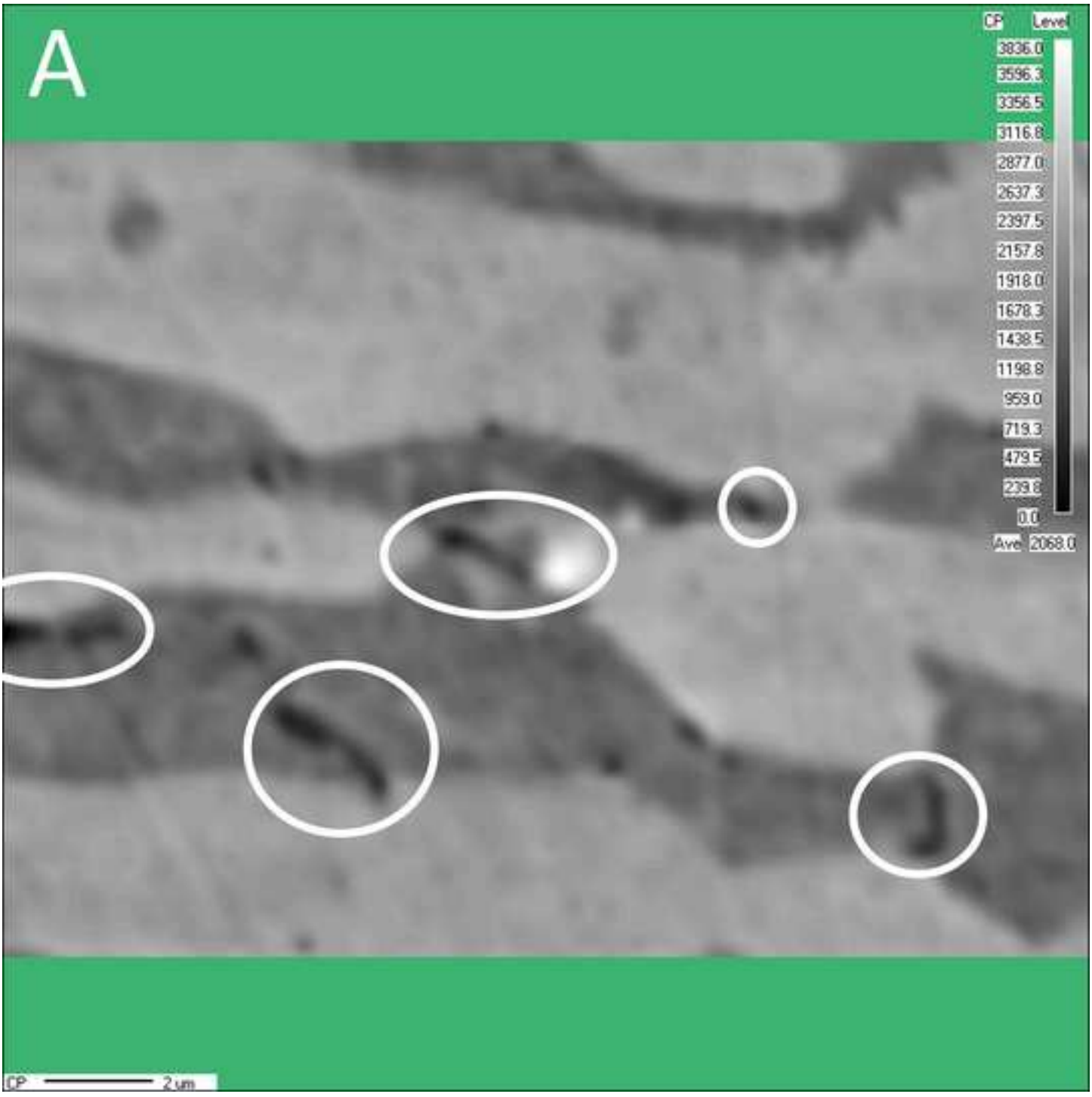

High-resolution Figure(s)
Click here to download high resolution image

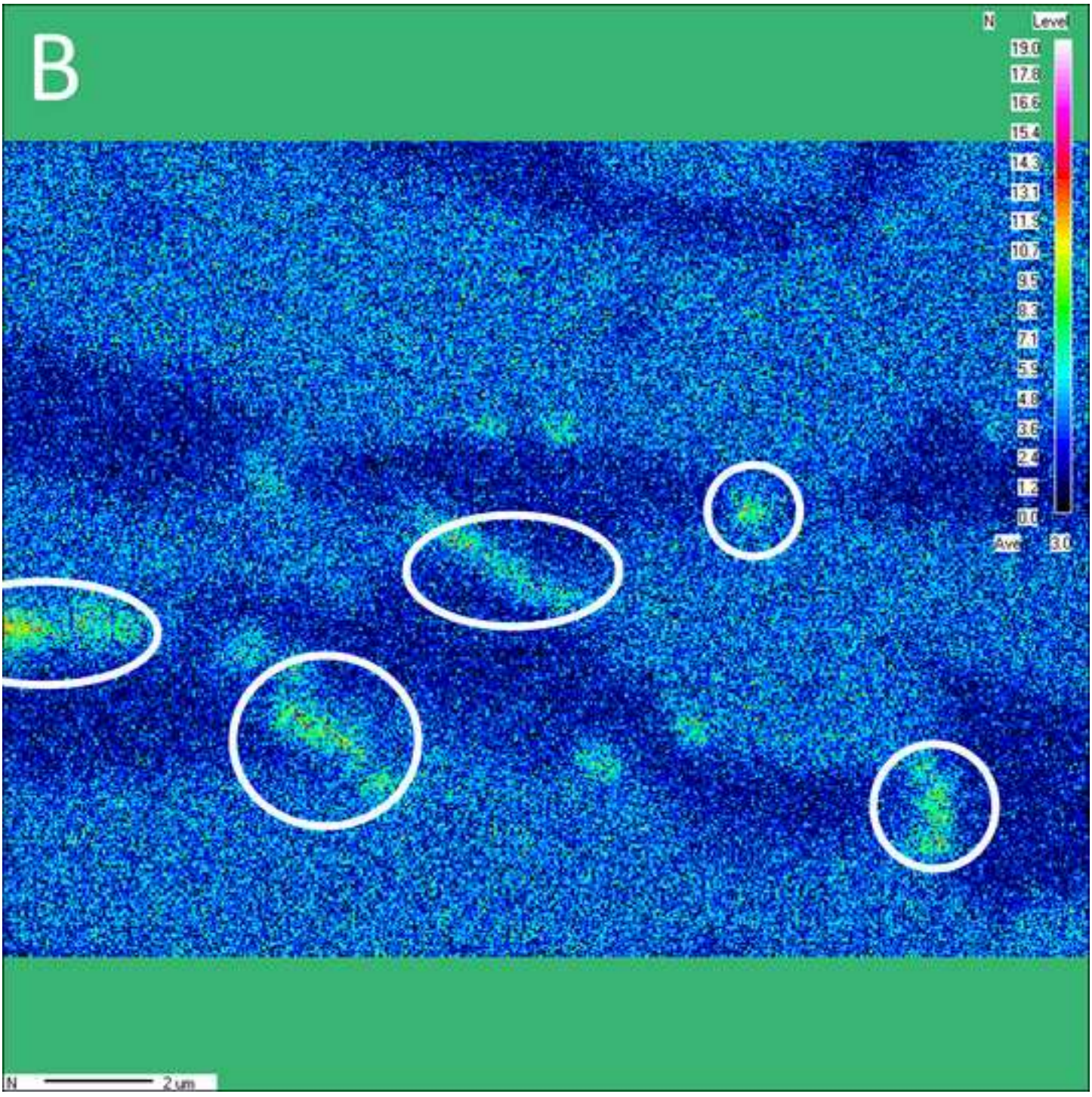

High-resolution Figure(s)
Click here to download high resolution image

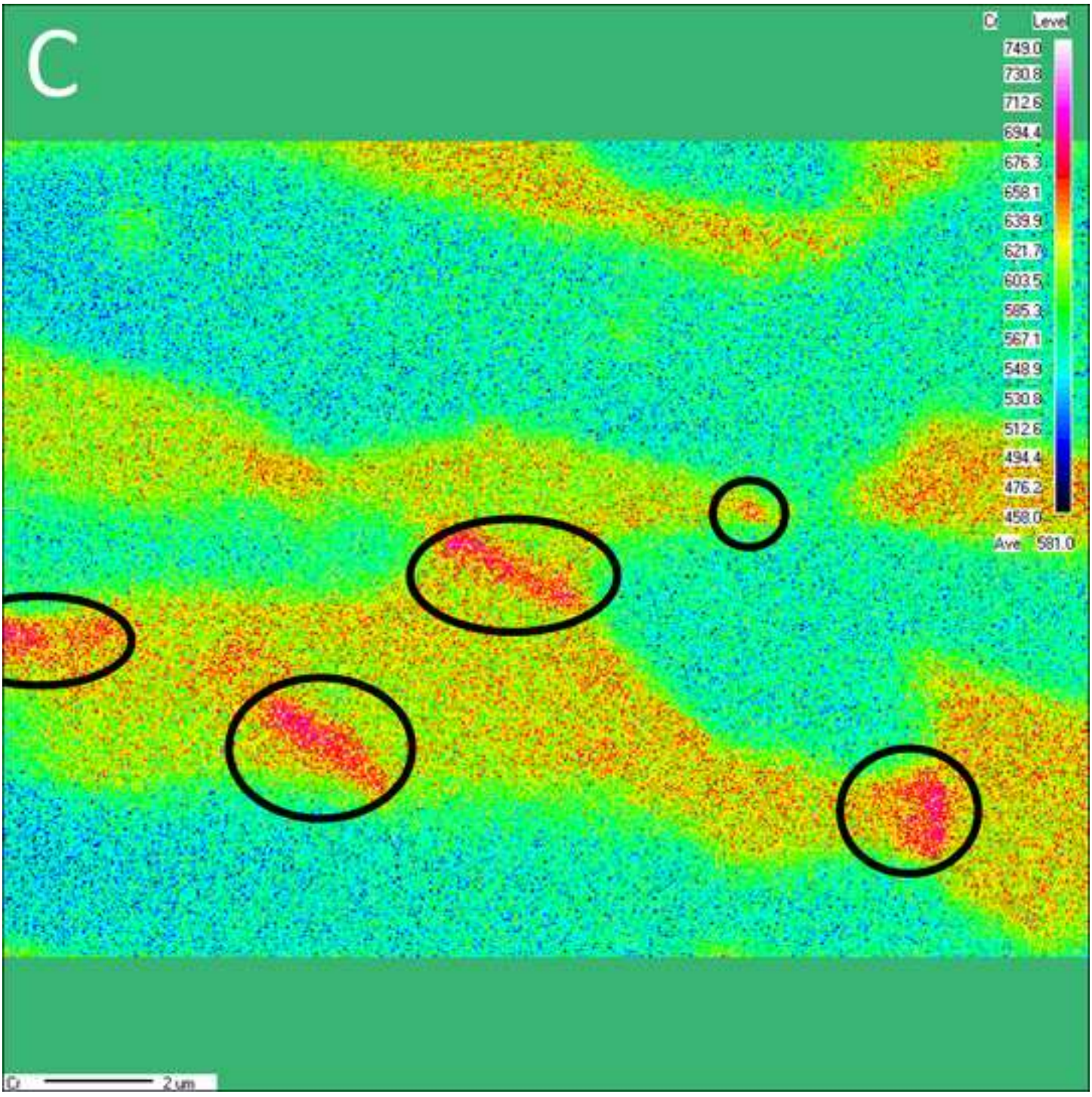

High-resolution Figure(s)
Click here to download high resolution image

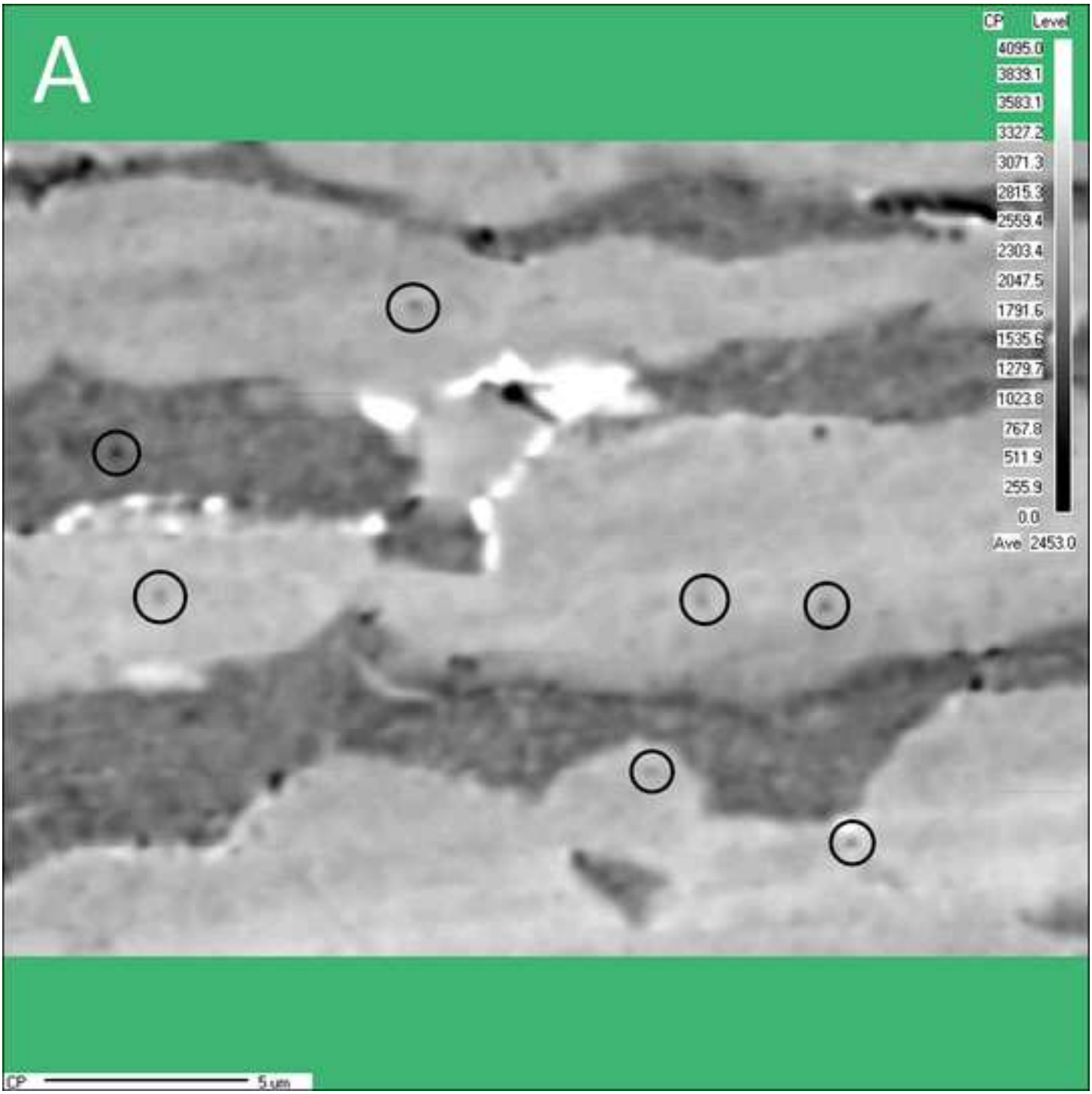

High-resolution Figure(s)
Click here to download high resolution image

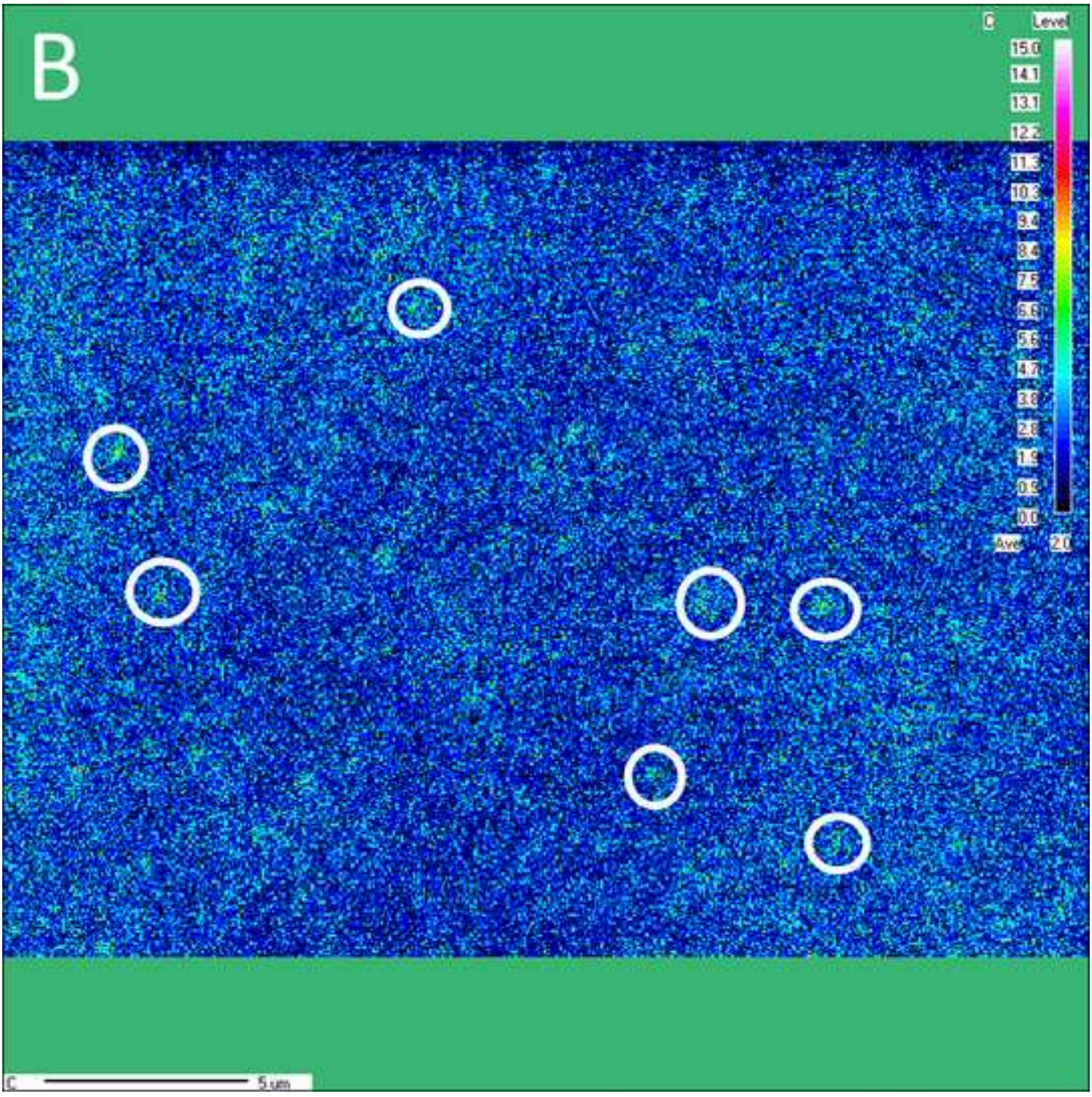

High-resolution Figure(s)
Click here to download high resolution image

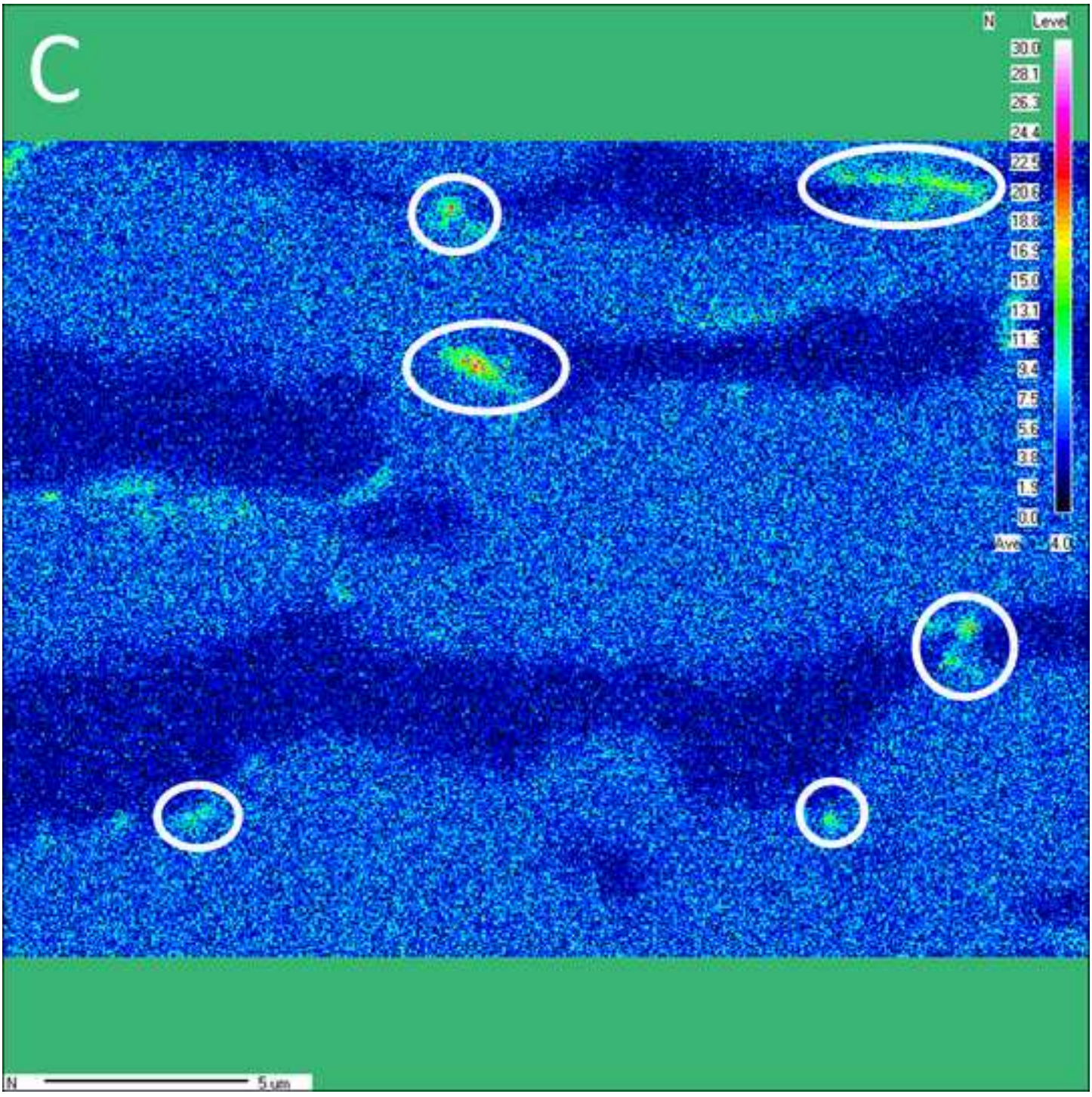

High-resolution Figure(s)
Click here to download high resolution image

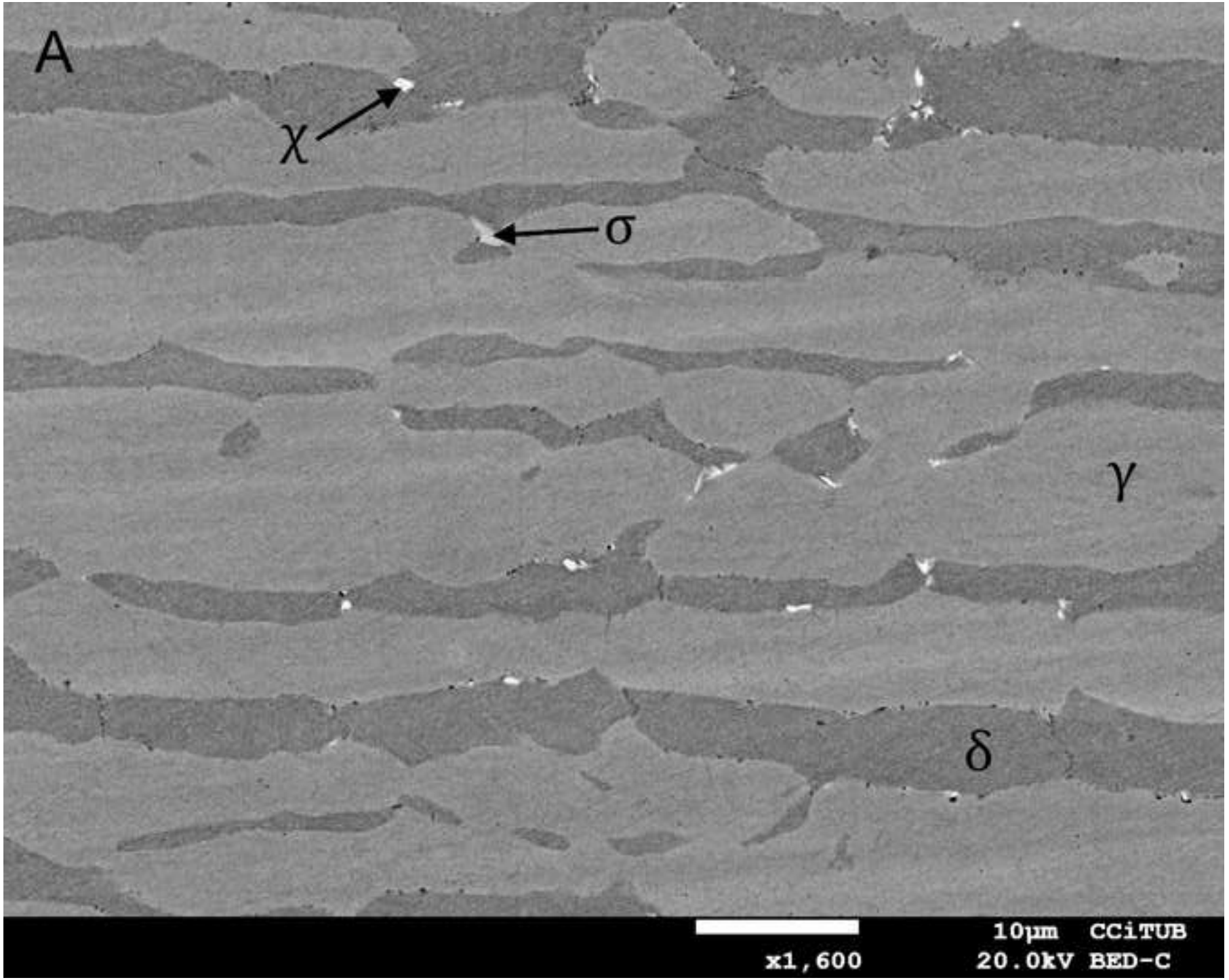

High-resolution Figure(s)
Click here to download high resolution image

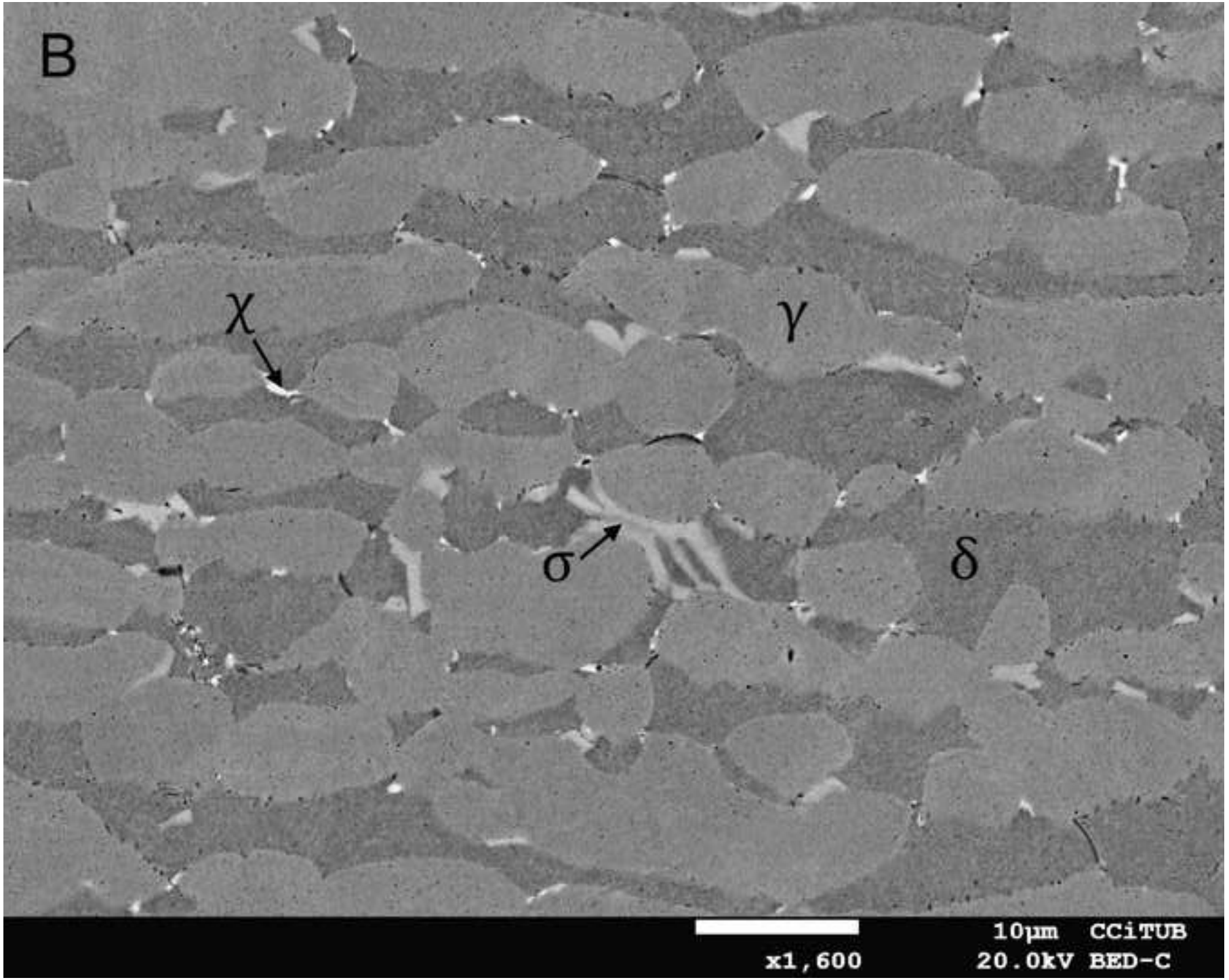

High-resolution Figure(s)
Click here to download high resolution image

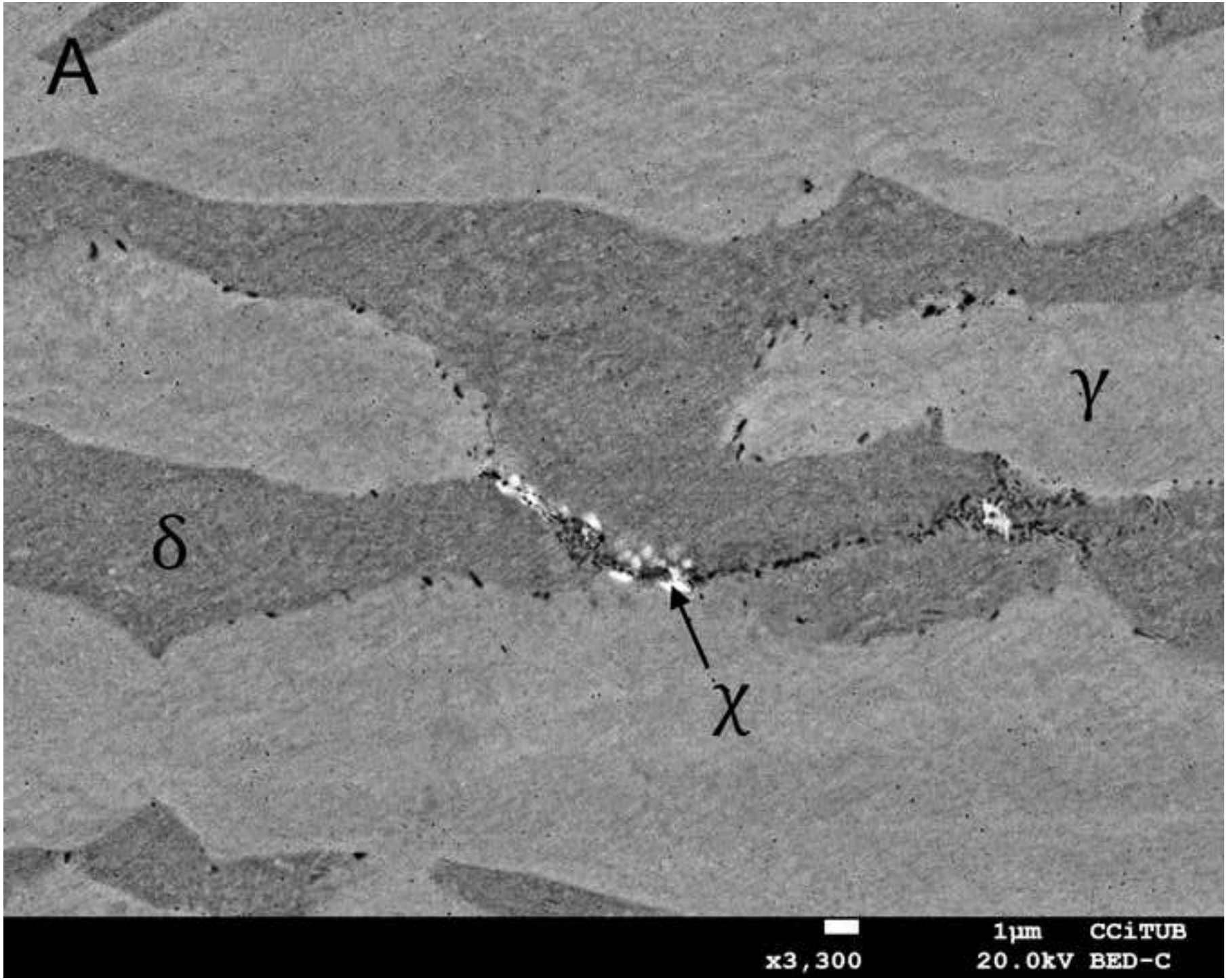

High-resolution Figure(s)
Click here to download high resolution image

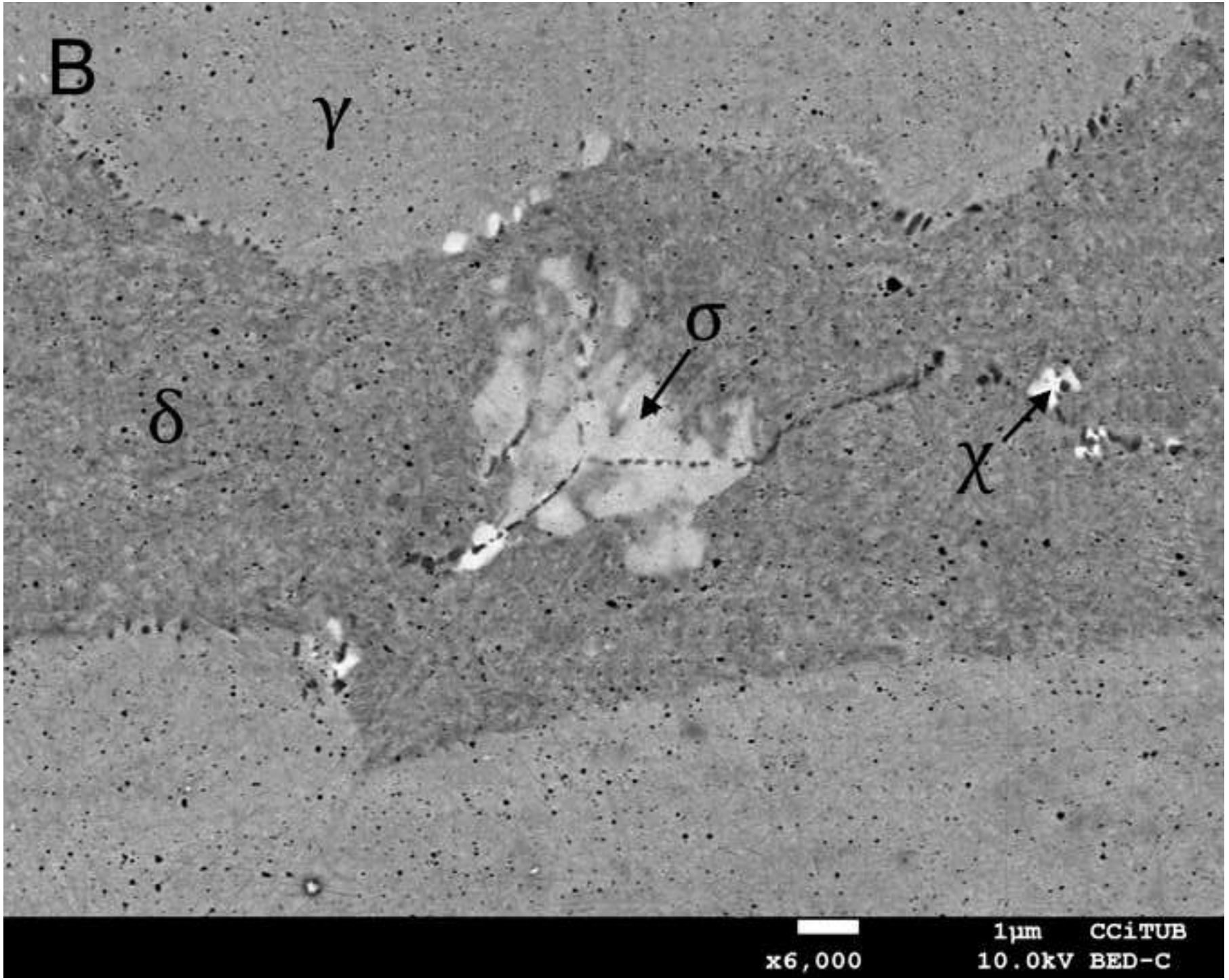

High-resolution Figure(s)
Click here to download high resolution image

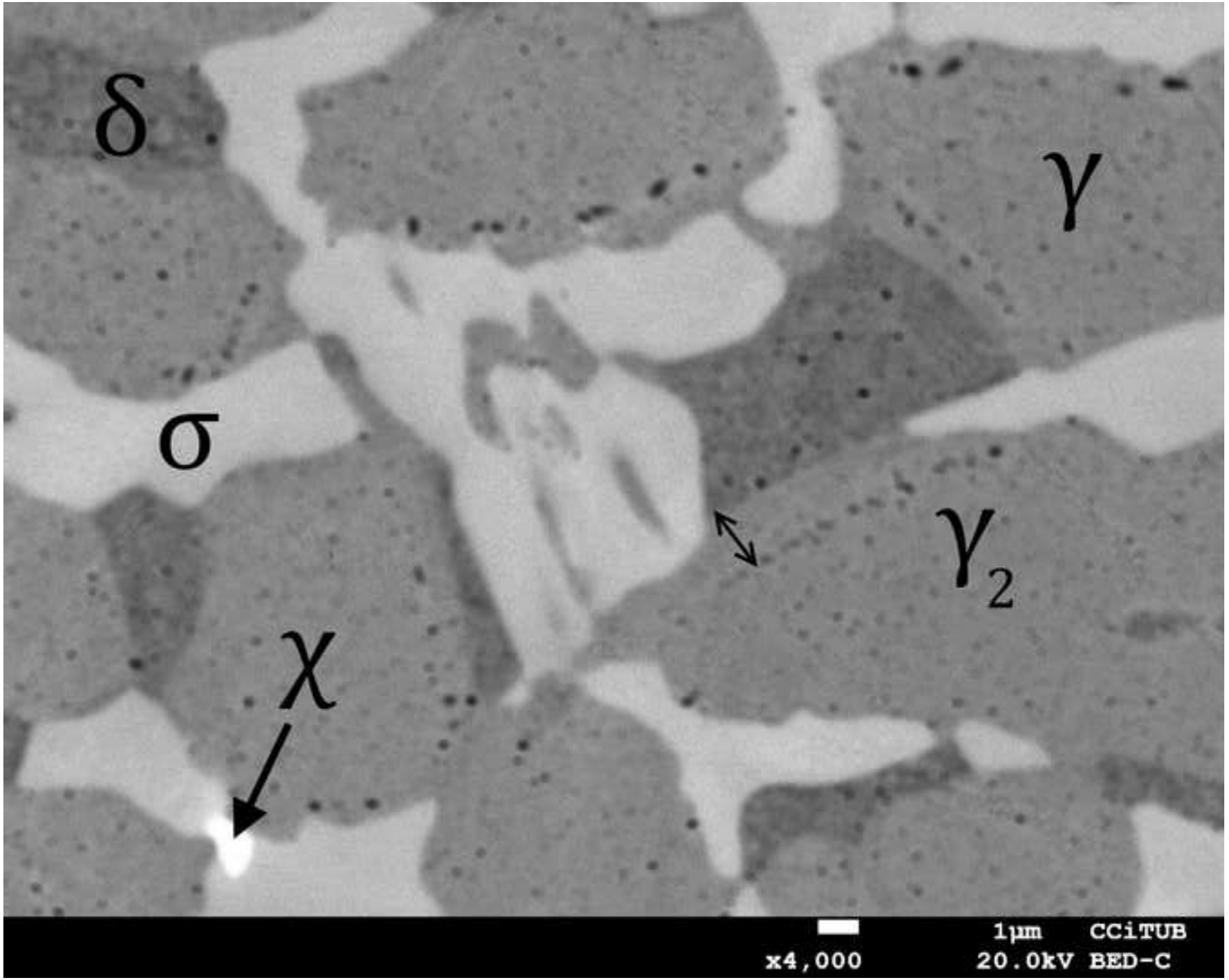

High-resolution Figure(s)
Click here to download high resolution image

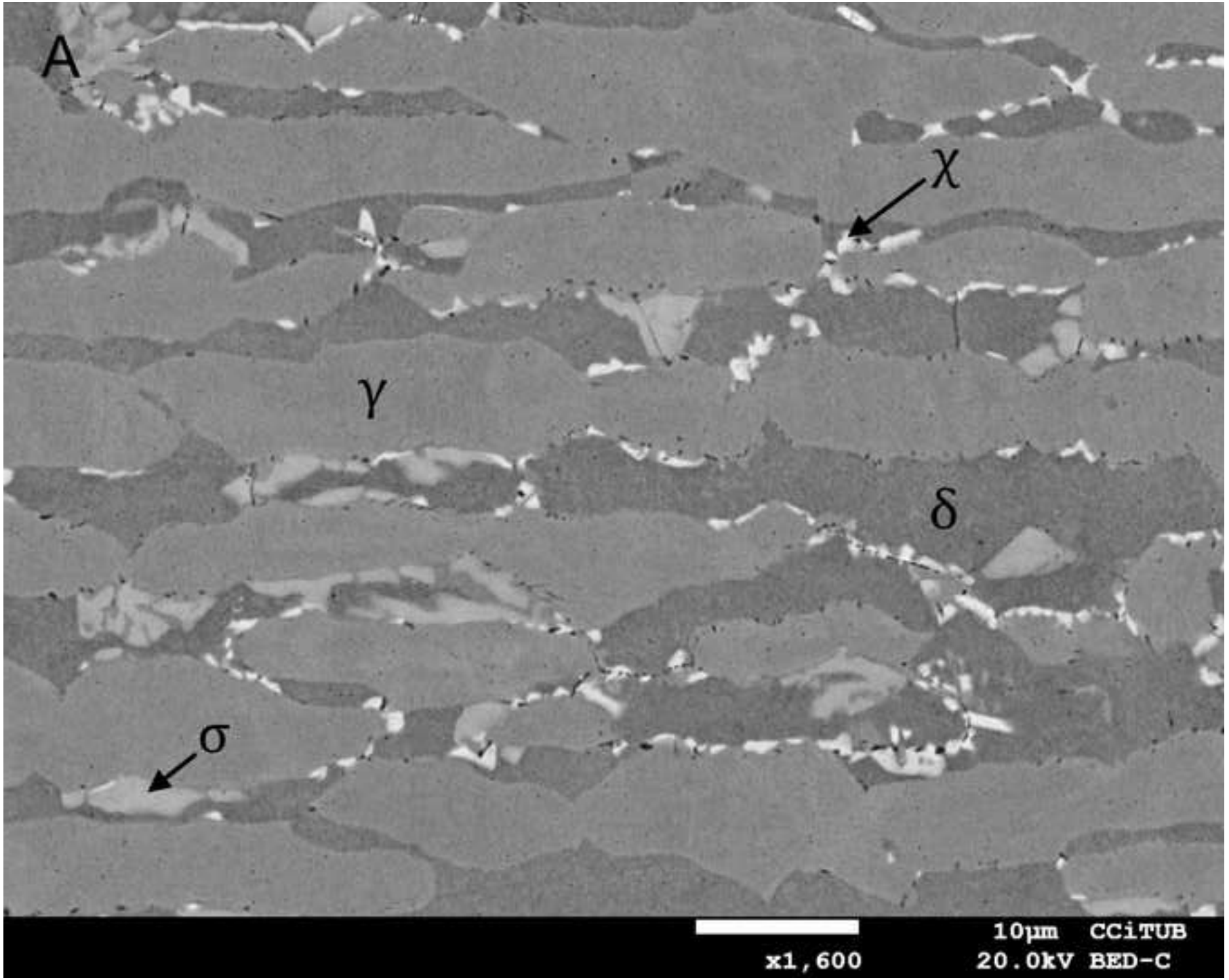

High-resolution Figure(s)

Click here to download high resolution image

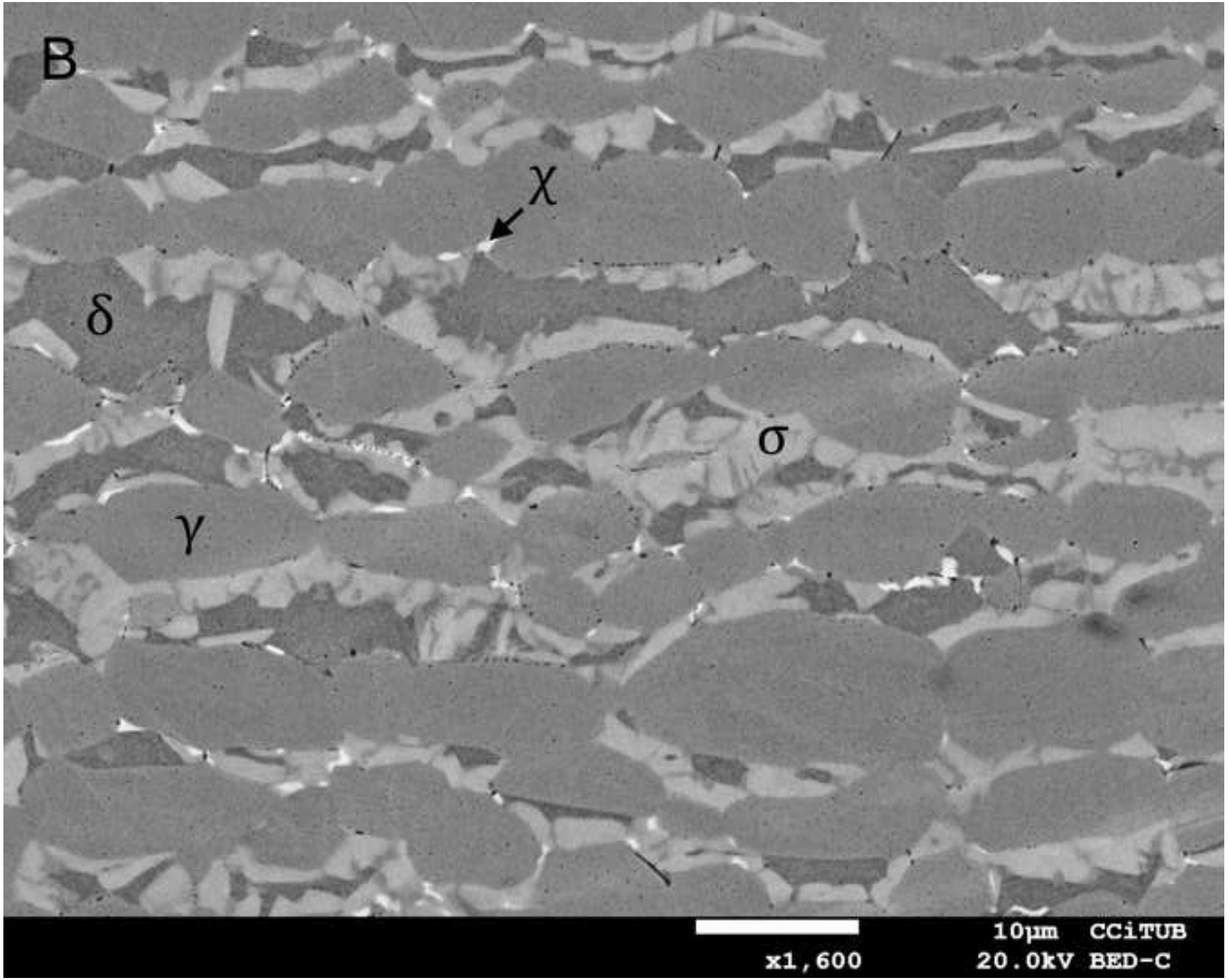

High-resolution Figure(s)

Click here to download high resolution image

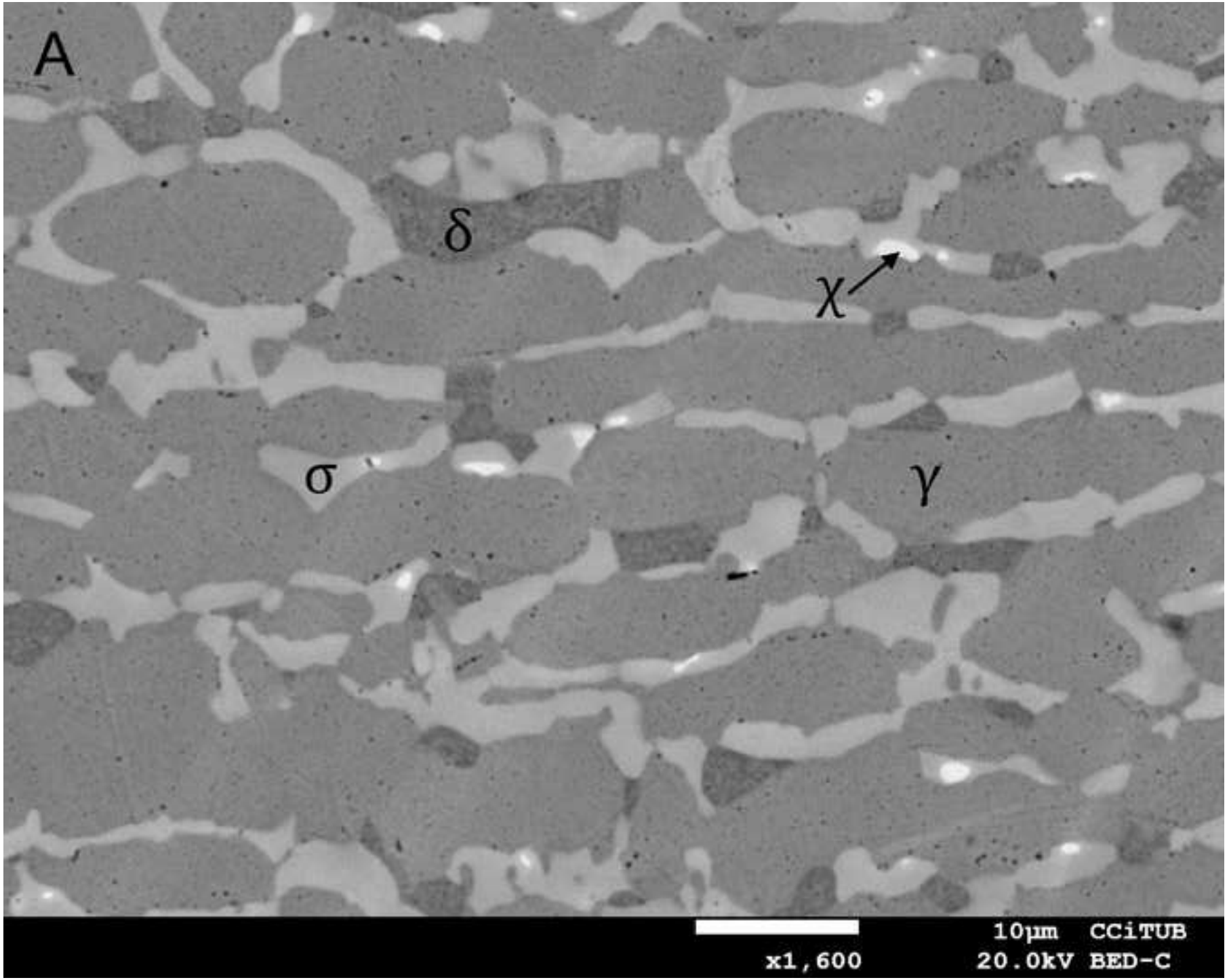

High-resolution Figure(s)
Click here to download high resolution image

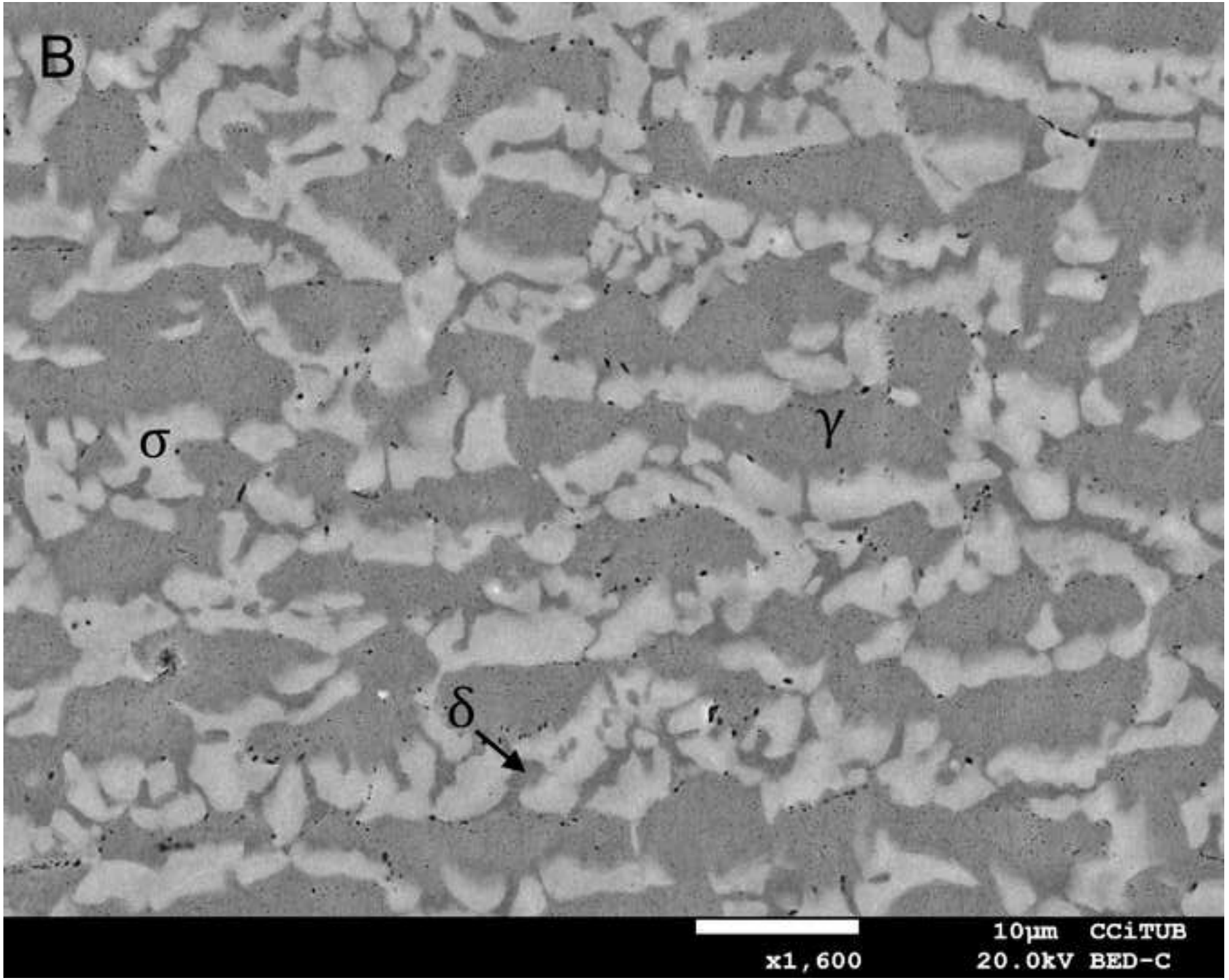

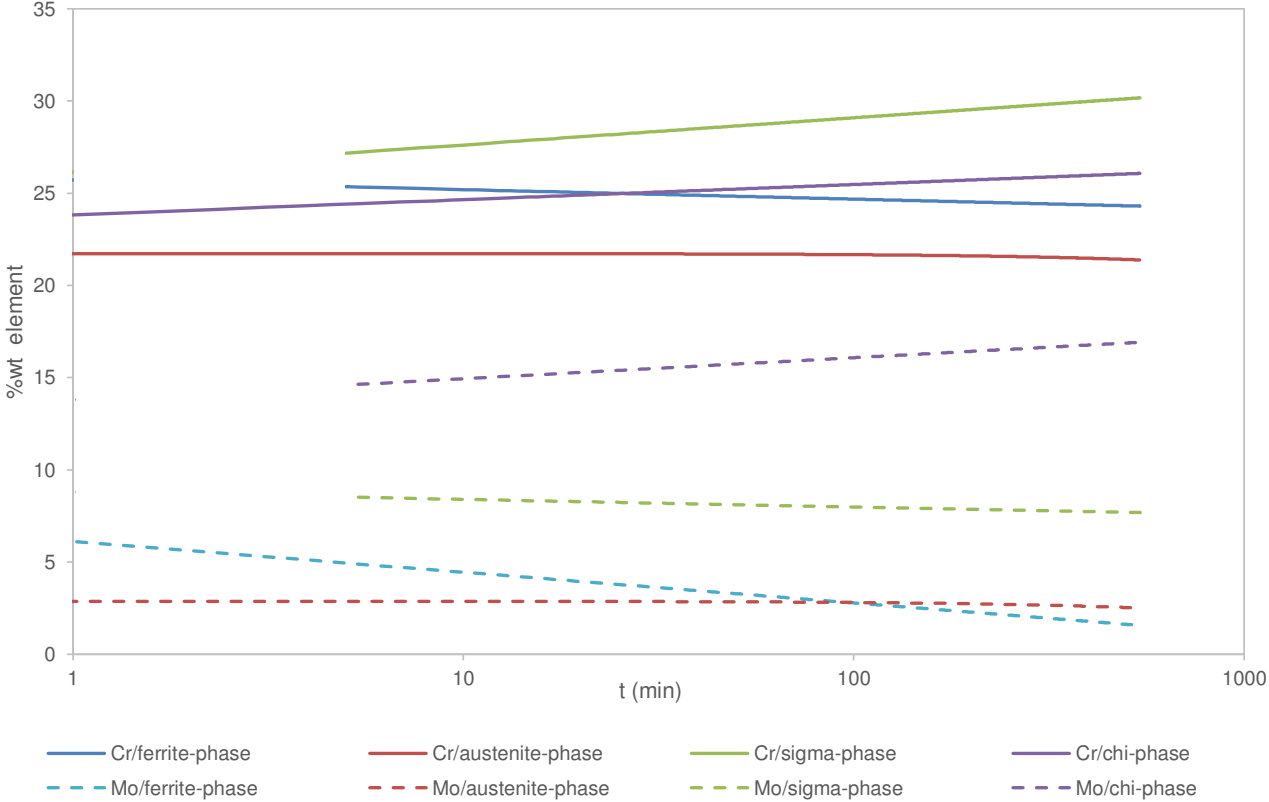
35
30
25
20
15
10
5
0
%wt element
1
10
100
1000
t (min)
Cr/ferrite-phase
Cr/austenite-phase
Cr/sigma-phase
Cr/chi-phase
Mo/ferrite-phase
Mo/austenite-phase
Mo/sigma-phase
Mo/chi-phase

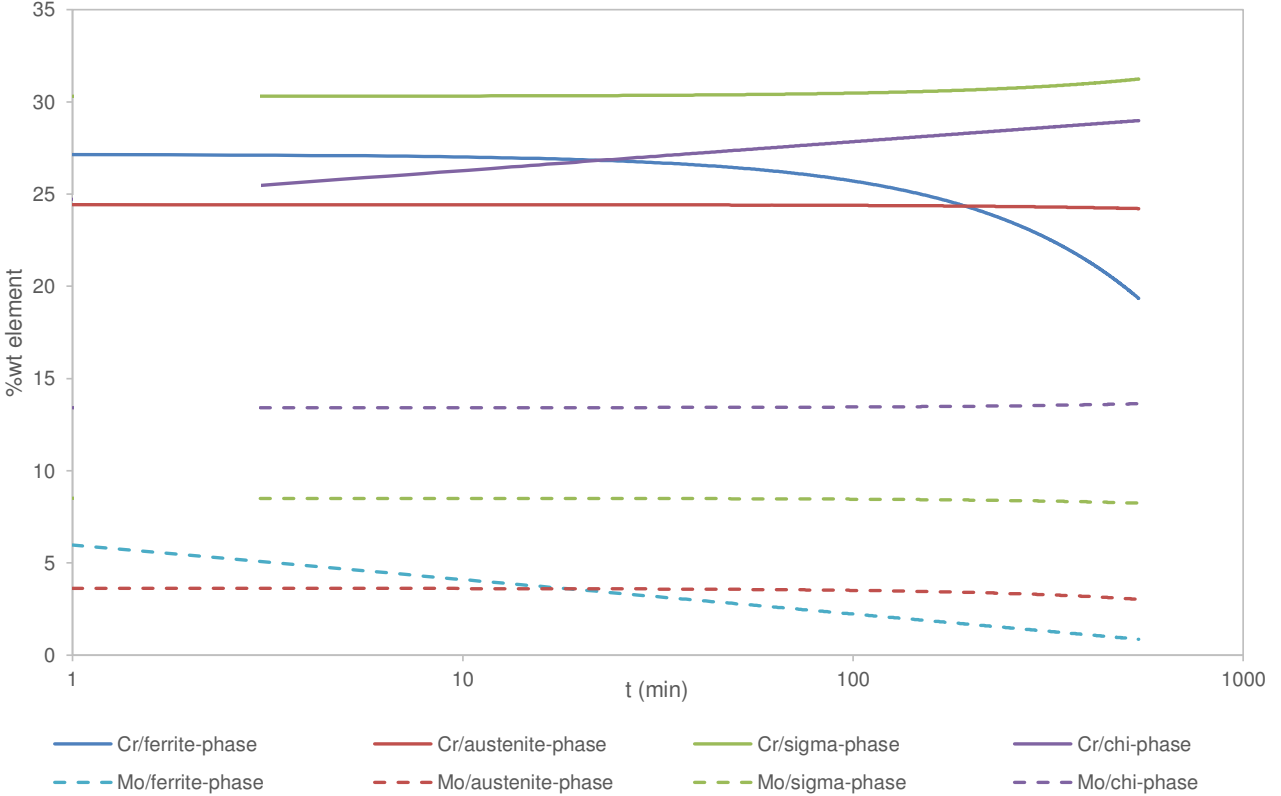
35
30
25
20
15
10
5
0
%wt element
1
10
100
1000
t (min)
Cr/ferrite-phase
Cr/austenite-phase
Cr/sigma-phase
Cr/chi-phase
Mo/ferrite-phase
Mo/austenite-phase
Mo/sigma-phase
Mo/chi-phase

High-resolution Figure(s)
Click here to download high resolution image

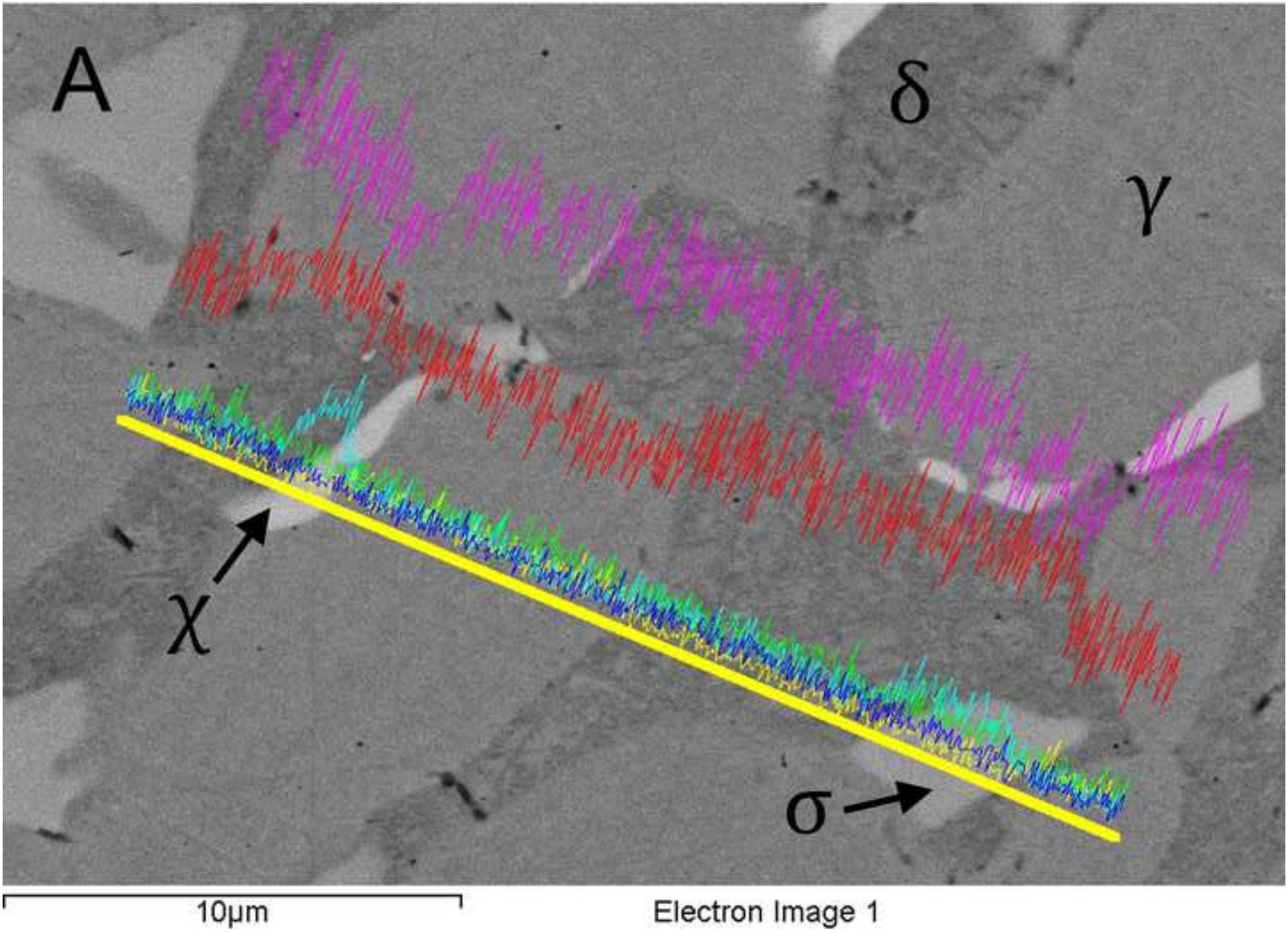

High-resolution Figure(s)

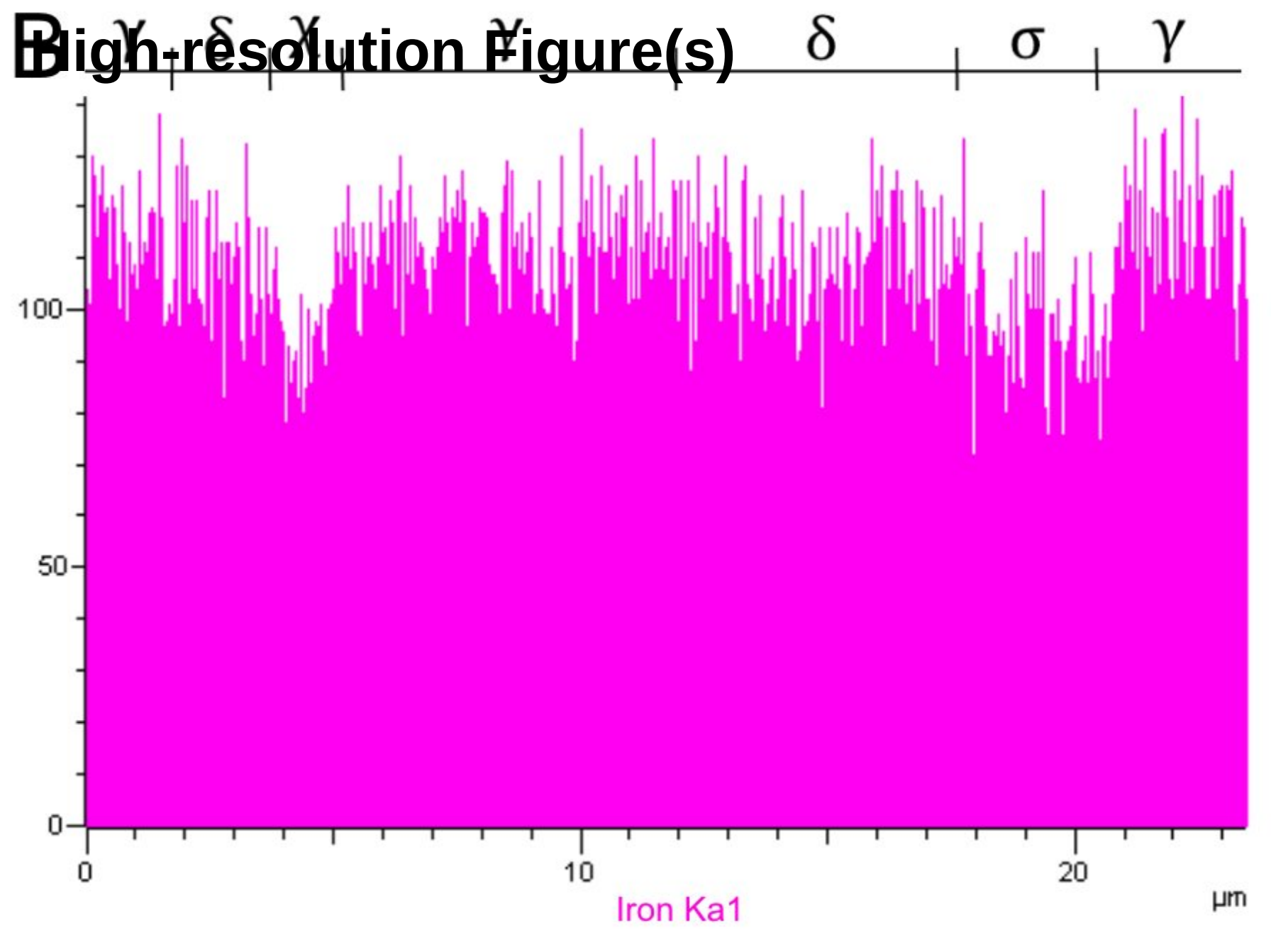

High-resolution Figure(s)

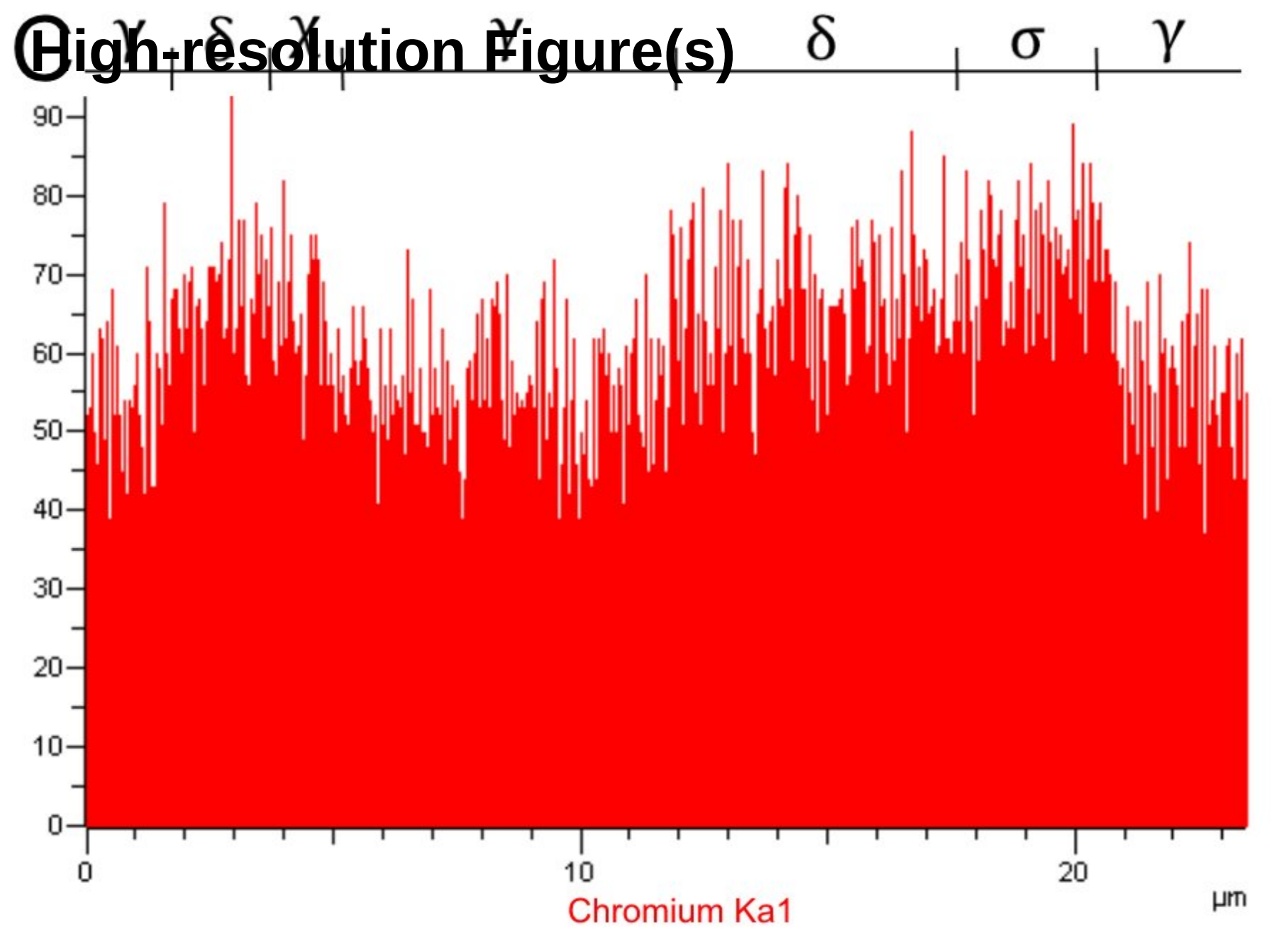

High-resolution Figure(s)

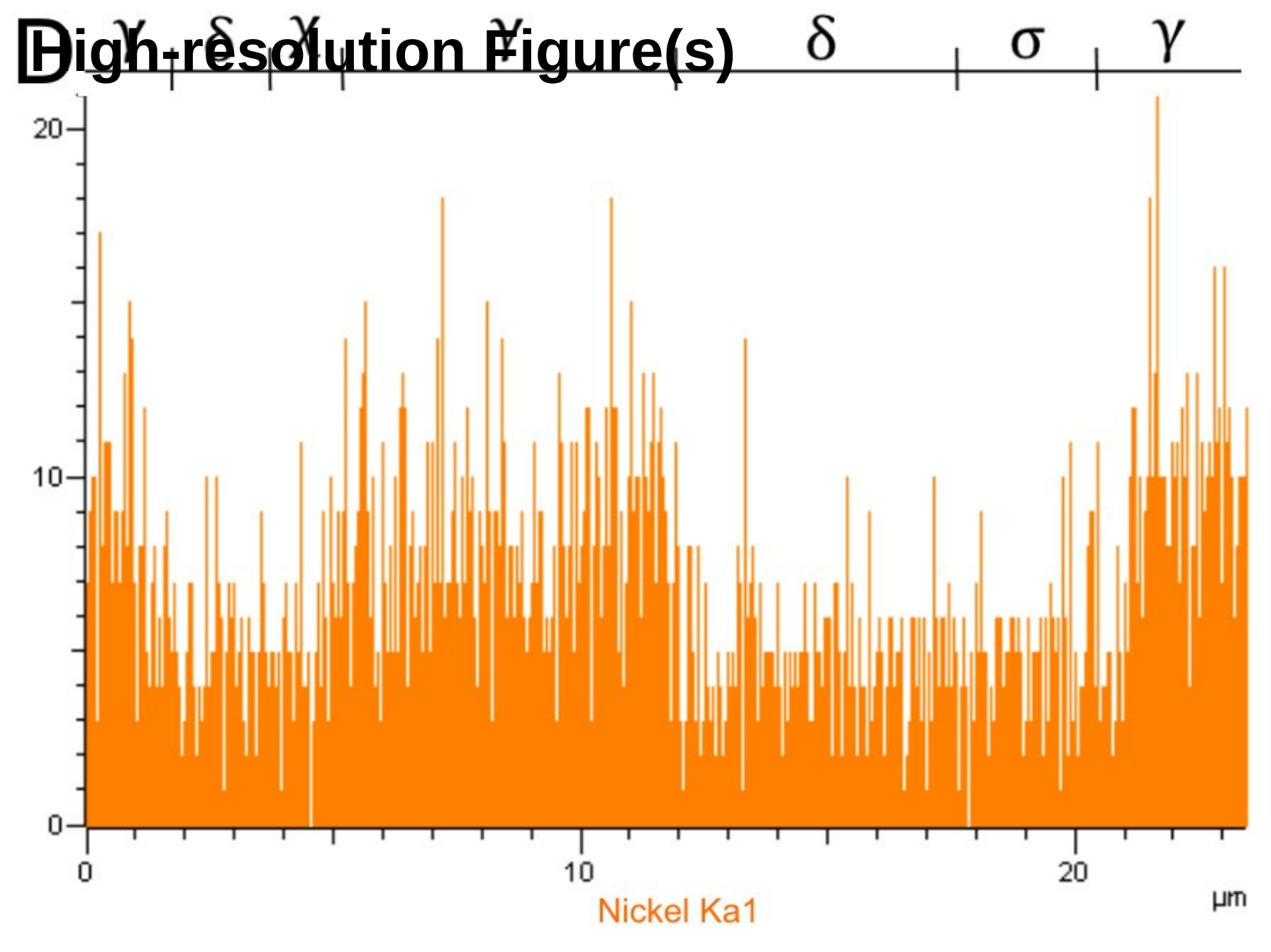

High-resolution Figure(s)

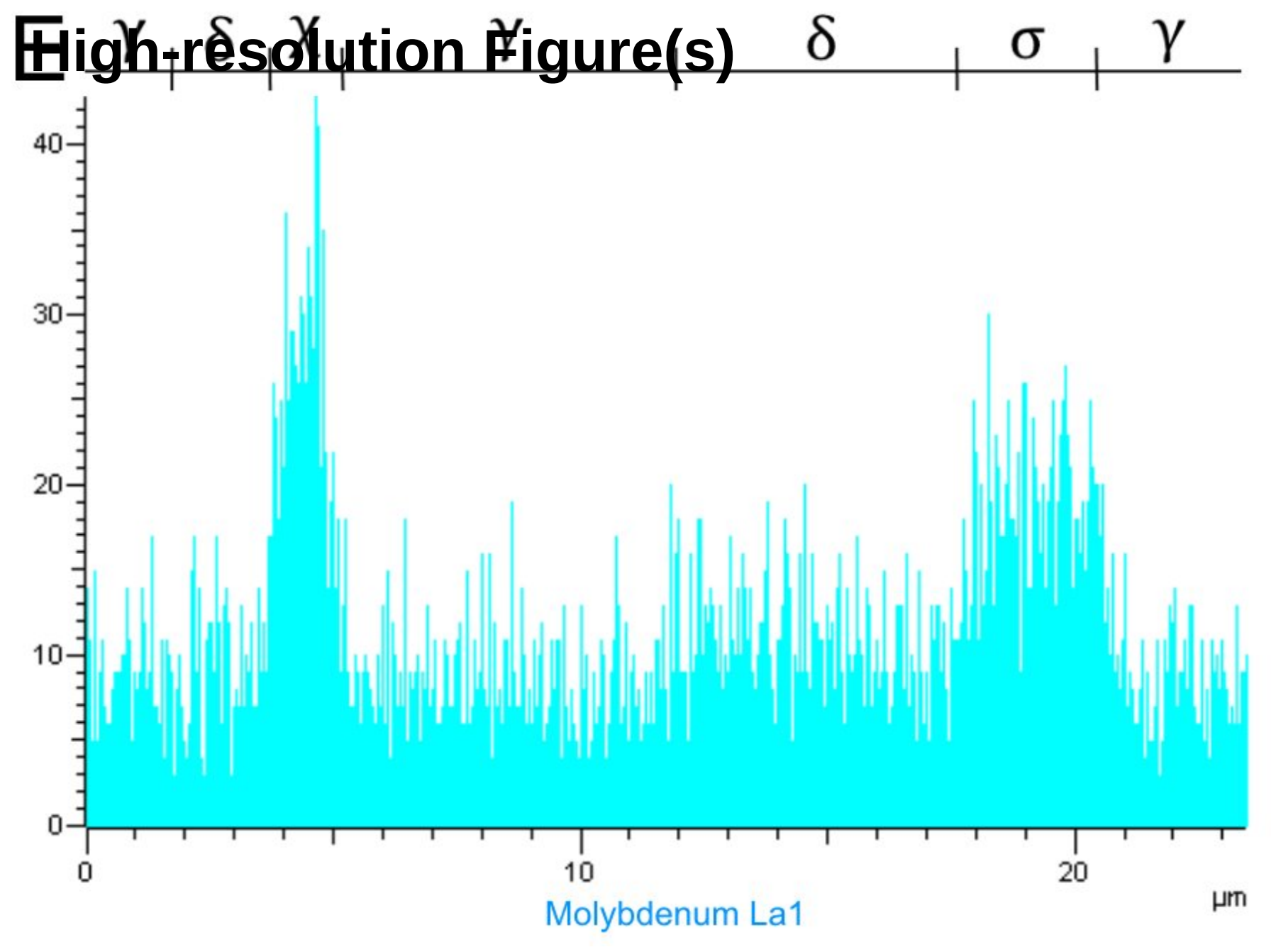

High-resolution Figure(s)

Click here to download high resolution image